Applied Energy 401 (2025) 126690

Contents lists available at ScienceDirect

Applied Energy

journal homepage: www.elsevier.com/locate/apenergy

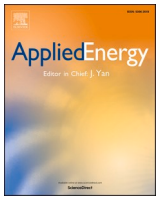

Numerical investigation of pulsed heating effects on MgH_2 desorption kinetics and thermal efficiency in solid-state hydrogen storage

Davoud Abdi Lanbaran [a,*], Pouria Farokhi Kojour [a], Chao Wang [a], Chuang Wen [b], Zhen Wu [c], Mi Tian [d], Bo Li [e,*]

[a] School of Engineering, University of Kent, UK
[b] School of Construction Management and Engineering, University of Reading, UK
[c] Department of Process Equipment and Control Engineering, Xi'an Jiaotong University, China
[d] Department of Chemical Engineering, University of Bath, UK
[e] School of Electrical, Electronic and Mechanical Engineering, University of Bristol, UK

HIGHLIGHTS

- A 15-min ON/OFF pulsed heating cycle reduces MgH_2 desorption time by 25 %, to 45 min with efficient desorption kinetics.
- Pulsed heating keeps the wall temperature below 661 K and retains 3.4 $kJ.m^{-3}$ of sensible heat, with improved thermal efficiency.
- Provide new insights into heat and mass transfer mechanism with pulsed heating and suggested reactor geometry.

ARTICLE INFO

Keywords:
Magnesium hydride (MgH_2)
Hydrogen desorption
Pulsed heat flux
ON/OFF cycle
Thermal efficiency

ABSTRACT

Magnesium hydride (MgH_2) offers high-capacity solid-state hydrogen storage, but it suffers from slow desorption due to its poor thermal conductivity. Here we model an MgH_2 composite containing 8 wt% expanded natural graphite (ENG), which raises the effective conductivity to 4.2 $W.m^{-1}.K^{-1}$. Finite element method (FEM) simulations performed in COMSOL Multiphysics compare a conventional constant radial heat flux with a stepwise ON/OFF (pulsed) regime. A 15-min ON/OFF cycle shortens the desorption time by 25 % from 60 to 45 min, keeps the wall temperature below 661 K, and leaves 3.4 $kJ.m^{-3}$ of recoverable sensible heat, whereas constant heating leaves none. Raising conductivity above 4.2 $W.m^{-1}.K^{-1}$ offers little extra benefit because gas-phase transport and surface kinetics then dominate. Pulsed heating also exploits thermal-conductivity-evolution feedback (TCEF): MgH_2 converts to metallic Mg during each pulse, further boosting conductivity and accelerating subsequent pulses. Heat-flux sequencing, therefore, delivers faster, more energy-efficient hydrogen release without internal heat-exchanger hardware, highlighting a simple path to improved thermal management in MgH_2-based composite storage systems.

1. Introduction

With increasing global energy demand, environmental concerns, and limitations of fossil fuels, hydrogen has emerged as one of the leading options for sustainable energy storage and transmission due to its high energy density, environmental friendliness, and potential for use in renewable energy generation [1,2]. The widespread adoption of hydrogen technologies depends on efficient and safe storage mechanisms. Among the available strategies, solid-state hydrogen storage, particularly in metal hydrides, offers significant advantages over gaseous and liquid hydrogen storage, including higher volumetric density, lower operating pressure, and improved safety characteristics [3]. This has led researchers to investigate various materials, including lithium-based compounds, sodium hydrides, and complex hydrides such as $LiAlH_4$ [4,5]. Among them, magnesium hydride (MgH_2) stands out from other options due to its favorable storage capacity, abundance, and relatively low cost [6]. However, its practical application is limited by inherent thermal management challenges, especially low thermal conductivity, and slow hydrogen desorption kinetics [7,8]. These challenges require targeted research to optimize the performance of this material.

* Corresponding authors.
E-mail addresses: da562@kent.ac.uk (D.A. Lanbaran), b.li@bristol.ac.uk (B. Li).

https://doi.org/10.1016/j.apenergy.2025.126690
Received 8 June 2025; Received in revised form 14 August 2025; Accepted 26 August 2025
Available online 1 September 2025

One of the primary barriers to utilizing magnesium hydride (MgH_2) as a hydrogen storage medium is its inherently low thermal conductivity [9]. The poor heat transport stems from a combination of factors: (i) its electrically insulating, defect-rich crystal lattice, which scatters heat-carrying phonons; and (ii) due to the highly porous and loosely packed nature of MgH_2 powders, thermal energy must propagate across numerous particle–particle interfaces, introducing considerable interfacial thermal resistance. [10,11]. These features hinder efficient heat transfer during the hydrogen desorption process, resulting in uneven temperature distribution, localized hot spots, or excessive reduction of the desorption rate under insufficient heat input [12,13]. When heated to the dehydrogenation range (300–400 °C), MgH_2 decomposes into metallic Mg and hydrogen gas. In the regions where this occurs, the metallic Mg exhibits a much higher thermal conductivity due to free-electron transport, with local values potentially exceeding 100 $W{\cdot}m^{-1}{\cdot}K^{-1}$ [14]. The phase change from MgH_2 to Mg increases the bed's thermal conductivity, creating a positive feedback loop: the initial desorption reaction rate (k) accelerates further heating and desorption. This phenomenon is referred to as Thermal Conductivity Evolution Feedback (TCEF) [15]. So far, numerous experimental and numerical efforts have been made to overcome these challenges, with the main goal being to increase the thermal conductivity and optimize the heat management in hydrogen desorption processes [16]. For example, Popilevsky et al. [17] showed that incorporating multi-walled carbon nanotubes (MWCNTs) into magnesium composites increased the thermal conductivity by approximately 20 %. Kumar et al. [18] also reported a significant improvement in heat transfer by embedding magnesium hydride in a 3D copper lattice structure. Furthermore, Yoshida et al. [19] experimentally confirmed that the increase in heat transfer, especially under convective heating, can significantly accelerate the hydrogen release kinetics. Therefore, improving heat transfer mechanisms, particularly through alternative thermal management strategies, is essential to overcoming the inherent conductivity limitations of this material, enhancing hydrogen storage efficiency, and achieving uniform temperature distribution in magnesium hydride-based systems [20].

Energy management remains a significant challenge for metal hydride (MH)-based hydrogen storage systems, especially for magnesium hydride (MgH_2), due to its intrinsically low thermal conductivity and high activation energy required for hydrogen desorption [21]. To overcome these limitations, passive strategies such as integrating phase change materials (PCMs) [22], thermochemical energy storage systems [23], and composite materials have been extensively investigated [24]. Ye et al. [25] demonstrated that incorporating PCMs into MgH_2 systems markedly enhances heat transfer and efficiently recycles reaction heat, reducing the overall energy requirement during hydrogen desorption. Similarly, Shi et al. [26] reported remarkable improvements in energy efficiency and thermal management through integrating thermochemical heat storage materials into metal hydride reactors. Innovative composite configurations, including multilayer designs using expanded natural graphite, have also shown promising enhancements in thermal conductivity, thus significantly improving overall energy efficiency [27]. However, these passive strategies, although beneficial for energy consumption, are generally limited in their ability to accelerate the hydrogen desorption rate, leaving a clear gap for methods that address both energy management and rapid hydrogen kinetics simultaneously [28].

Active thermal-management measures, including compact spiral or shell-and-tube heat exchangers that boost heat-transfer area [29,30], radial or longitudinal fins that extend the conduction path through the bed [31], and high-conductivity inserts such as metallic wire matrices or open-cell metal foams [32,33] reduce internal thermal resistance, narrow temperature gradients to within a few kelvin, and shorten MgH_2 desorption times by up to an order of magnitude compared with passive beds [34]. Elman et al. [35] for instance, demonstrated through numerical and experimental analyses that radial fins embedded within magnesium-based hydrogen storage reactors can reduce hydrogen desorption time by approximately 63 %, thanks to enhanced thermal conductivity and increased heat transfer surface area. Eisapour et al. [36] further highlighted the advantages of conical coil heat exchangers, achieving up to a 69 % reduction in hydrogen absorption and desorption times compared to conventional reactor designs. Nevertheless, these active methods introduce critical constraints, including increased system complexity, higher installation costs, and substantial reductions in available storage volume for MgH_2, thus limiting practical hydrogen storage capacity [37]. Additionally, Xu et al. [38] emphasized that the efficiency of active heat transfer methods like metal foams and fins typically declines as reactor size increases, posing scalability challenges. Consequently, there remains an urgent need for novel thermal management strategies capable of simultaneously optimizing energy consumption, hydrogen desorption speed, and thermal distribution uniformity without significantly complicating the system or reducing the effective hydrogen storage capacity, a gap that the present research on stepwise radial heat flux strategies specifically addresses.

Despite extensive research and numerous applications, traditional approaches to managing hydrogen desorption from magnesium hydride typically involve applying a constant radial heat flux through the vessel wall. Although this method is simple and commonly used, it often results in poor thermal management, energy waste, and inefficient heat penetration into the deeper layers of the hydride bed due to the material's inherently low thermal conductivity. To address these limitations and bridge the gap between energy efficiency and desorption acceleration, the present study proposes and numerically investigates a novel strategy based on stepwise (ON–OFF) radial heat flux. Unlike conventional constant-flux methods, the stepwise approach is designed to improve thermal penetration, minimize local hot spots, and optimize energy input for efficient hydrogen desorption. To the best of the authors' knowledge, this work is the first to demonstrate that a pulsed heat input can simultaneously accelerate hydrogen release and improve thermal efficiency in MgH_2 systems, an achievement not reported in previous studies. Using a comprehensive finite element analysis, this research evaluates temperature distribution, desorption kinetics, thermal gradients, and energy efficiency under various heat flux strategies. The concept of "heat flux sequencing" introduced here not only simplifies reactor design by eliminating the need for internal heat exchangers but also provides a thermally adaptive solution well-suited for integration with intermittent renewable heating sources. While the simulation results are promising, experimental validation will be necessary to confirm the feasibility of implementing this method in practice. The outcomes of this numerical investigation provide new insights that can support future experimental design and advance the practical deployment of MgH_2-based storage systems.

2. Methodology

2.1. Geometry and material description

In this study, numerical simulations were performed to investigate the hydrogen desorption behaviour of magnesium hydride (MgH_2) using the COMSOL Multiphysics software based on the finite element method (FEM). These simulations aimed to evaluate the efficiency and effectiveness of two different constant radial heat flux and stepwise (ON/OFF pulsed) strategies. For a coherent analysis and meaningful comparison, a single 2D symmetric geometry (as shown in Fig. 1) was used to simulate two distinct heat flux strategies, referred to here as Fig. 1(a) and Fig. 1 (b). To clarify the rationale for using numerical simulation instead of experiments, it should be noted that performing an extensive parametric study of heating strategies experimentally would be time-consuming, costly, and limited by instrumentation constraints. Therefore, finite element modeling provides an efficient and practical method for exploring various heat flux conditions and evaluating their performance in a controlled and replicable manner. The simulated bed is a composite of MgH_2 mechanically mixed with 8 wt% expanded with natural

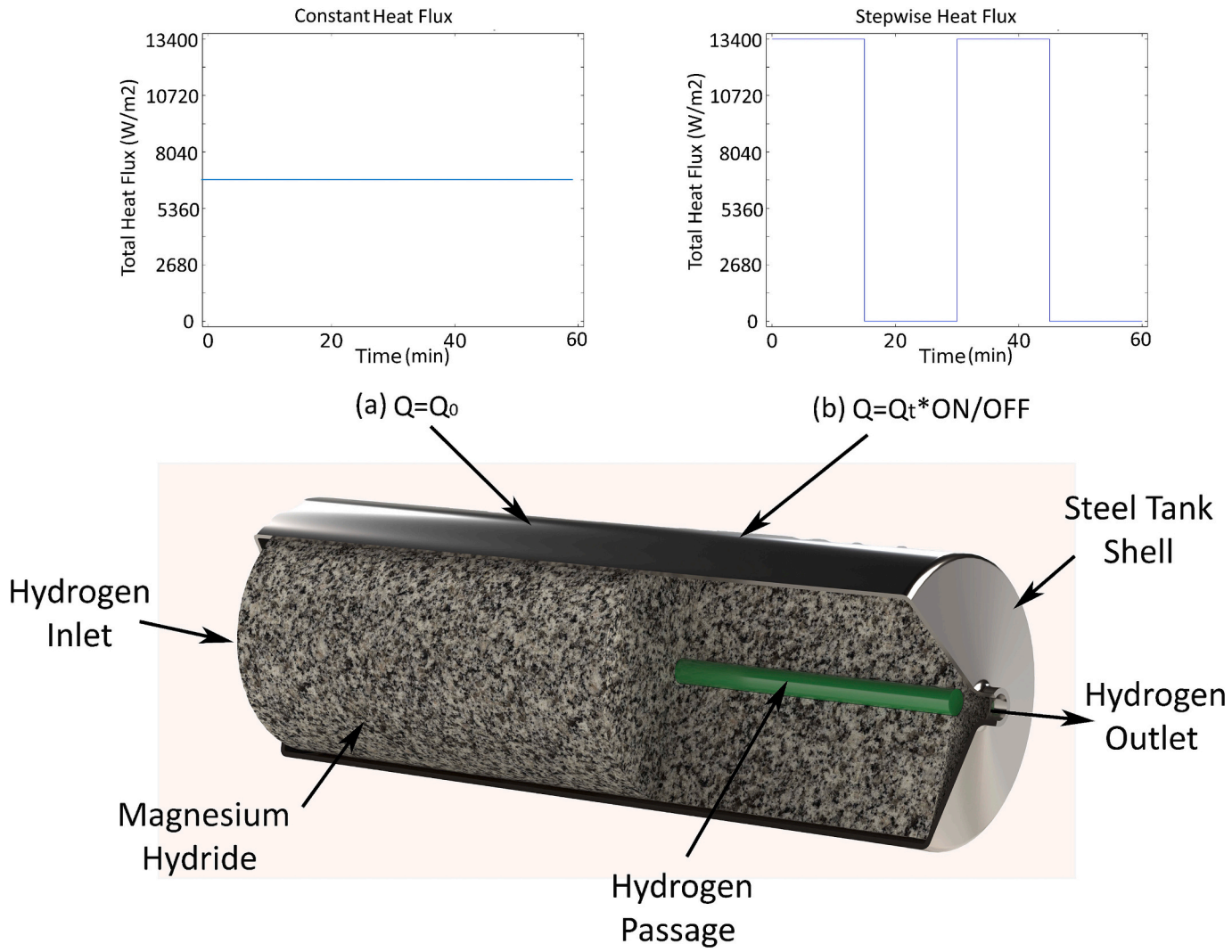

Fig. 1. A Schematic geometry for hydrogen desorption under various heat fluxes (a) Constant (b) Stepwise.

graphite (ENG). The ENG additive raises the effective thermal conductivity by almost an order of magnitude, a key requirement for accurate heat-transfer modeling.

Geometry 1(a) represents the traditional approach by applying a constant radial heat flux, where heat is applied continuously and uniformly through the external tank wall, similar to the thermal management methods commonly used in MgH_2-based hydrogen storage systems. In contrast, geometry 1(b) shows a cylindrical tank containing magnesium hydride (MgH_2) whose external wall is subjected to a square-wave heat flux pulse (ON-OFF). In each "ON" half-cycle, the wall supplies the energy required to carry out the endothermic hydrogen-releasing reaction, and in each "OFF" half-cycle, the heat input is stopped to allow the accumulated heat to be distributed deeper into the bed before the wall region becomes too hot. Both strategies consist of a porous magnesium hydride bed surrounding a central hydrogen gas outlet path to accurately model the heat and mass transfer dynamics, and realistic and consistent boundary conditions, including fixed boundary surfaces, conductive heat transfer boundaries, and hydrogen gas outlet conditions, are assumed for both methods. Also, key parameters such as initial temperature, hydrogen gas flow rate, and heat flux intensity are kept constant in both geometries to allow for accurate and meaningful comparison. The physical and thermal properties used in the simulation, including density, thermal conductivity, and specific heat capacity, are extracted from reliable data and previous experimental studies and are comprehensively presented in Table 1. To acknowledge modeling simplifications, the effective thermal conductivity of the hydride bed is held constant at 4.2 $W{\cdot}m^{-1}{\cdot}K^{-1}$, which corresponds to the baseline value for MgH_2.

By systematically comparing two distinct radial heat flux strategies within the same geometric framework, this study provides valuable insights into thermal management optimization, and its findings can significantly improve the hydrogen desorption performance and energy efficiency in magnesium hydride-based storage systems.

2.2. Governing equations

In this study, the numerical analysis of hydrogen desorption from magnesium hydride (MgH_2) is carried out by solving the governing equations of heat transfer and fluid dynamics in porous media. These core equations include the energy conservation equation, mass conservation equation, chemical reaction kinetics, hydrogen gas flow (described by Darcy's law), and a periodic heat flux model that simulates the thermal behaviour and removal kinetics in the MgH_2 tank.

- Heat transfer equation:

The heat transfer process in the MgH_2 tank is controlled by the energy conservation equation, which is expressed as follows [20]:

Table 1
Thermophysical Properties of Materials.

Description	Symbol	Value	Parameter
Initial Pressure [8]	P_0	0.1 MPa	Initial hydrogen pressure in MgH_2
Porosity [20]	ε	0.32	Porosity of MgH_2 bed
Hydrogen storage capacity [20]	w_{H_2}	6 %	Maximum hydrogen-to-metal mass ratio for MgH_2
Density of Magnesium Hydride [8]	ρ_{MgH_2}	1450 kg/m3	Density of MgH_2
Reaction Enthalpy [20]	$\Delta H_{desorption}$	75 kJ/mol	Reaction enthalpy of MgH2 dehydrogenation
Molar Mass of Hydrogen [20]	M_{H_2}	2.016 g/mol	Molar mass of H_2
Molar Mass of Magnesium Hydride [20]	M_{MgH_2}	26.3209 g/mol	Molar mass of MgH_2
Molar Mass of Magnesium [20]	M_{Mg}	24.3050 g/mol	Molar mass of Mg
Effective Thermal Conductivity of Magnesium Hydride with (ENG) [23]	λ_{MgH_2}	4.2 W/m·K	Heat transfer capability of MgH_2
Specific Heat Capacity of Magnesium Hydride [23]	C_{PMgH_2}	1250 J/kg·K	Heat capacity of MgH_2
Thermal Conductivity of Hydrogen [17]	λ_{H_2}	0.168 W/m·K	Heat transfer in gaseous hydrogen
Specific Heat Capacity of Hydrogen [17]	C_{PH_2}	14200 J/kg·K	Heat capacity of hydrogen gas
Activation Energy [20]	E_a	41 kJ/mol	Activation energy for hydrogen desorption
Arrhenius Pre-exponential Factor [8]	A	10 1/s	Arrhenius reaction rate parameter
Hydrogen Volume Fraction at $t = 0$	x_{H_2}	1.0	MgH_2 tank is fully saturated with H_2 at t = 0
Diameter of Central Manifold	d_h	1 mm	Central axial hydrogen outlet (manifold)
Diameter of Metal Hydride Bed	d_m	4 mm	Full diameter of the magnesium hydride cylindrical domain
Length of Metal Hydride Bed	l_m	1 m	Full length of the magnesium hydride domain

$$(\rho C_P)_{eff}\frac{\partial T}{\partial t} + (\rho C_P)\mathbf{u}.\nabla T = \nabla\cdot(\lambda\nabla T) + \dot{Q} \tag{1}$$

where $(\rho C_P)_{eff}$ represents the effective heat capacity ($J.m^{-3}\cdot K^{-1}$), (ρC_P) is the fluid's heat capacity ($J.m^{-3}\cdot K^{-1}$), **u** is fluid velocity ($m.s^{-1}$), λ is the effective thermal conductivity ($W\cdot m^{-1}\cdot K^{-1}$), and $\dot{Q}$ is the volumetric heat generation rate ($W.m^{-3}$). The effective heat capacity incorporates the weighted heat capacities of solid and fluid phases based on the porosity.

- Hydrogen Desorption Kinetics:

The hydrogen desorption kinetics from magnesium hydride is described using a modified Arrhenius Eq. [39]:

$$\frac{dx}{dt} = k\left(\frac{P}{P_{eq}} - 1\right) \tag{2}$$

where x is the reacted fraction, k is reaction rate ($1.s^{-1}$) is given by:

$$k = A\cdot\exp\left(\frac{-E_a}{RT}\right) \tag{3}$$

where A is the Arrhenius coefficient ($1.s^{-1}$), $-E_a$ is activation energy ($J.mol^{-1}$), R is the gas constant ($8.314\ J.mol^{-1}.K^{-1}$), and T is temperature (K).

- Mass Conservation of Hydrogen:

Mass conservation for hydrogen within the porous MgH_2 structure is expressed through the continuity Eq. [40]:

$$\frac{\partial\rho}{\partial t} + \nabla\bullet(\rho u) = S \tag{4}$$

where ρ is density ($kg.m^{-3}$), u is the hydrogen velocity ($m.s^{-1}$), and S is the source term from the desorption reaction.

- Equilibrium Pressure Model:

The equilibrium pressure of hydrogen in the system is determined using the Van't Hoff Eq. [41]:

$$P_{eq,H_2} = P_{ref}\times\exp\left(\left(\frac{\Delta H_r}{RT}\right) - \left(\frac{\Delta S_r}{R}\right)\right) \tag{5}$$

where P_{eq,H_2} is equilibrium pressure (Pa), P_{ref} is reference pressure (typically 1 atm),ΔH_r is the enthalpy change ($J.mol^{-1}$), and ΔS_r is the entropy change ($J.mol^{-1}.K^{-1}$).

- Hydrogen Transport in Porous Media:

Darcy's law describes hydrogen diffusion within the porous metal hydride medium:

$$\mathbf{v} = -\frac{\kappa}{\mu}\nabla P \tag{6}$$

where **v** is the hydrogen velocity ($m.s^{-1}$), κ is permeability (m^2), μ is hydrogen dynamic viscosity ($kg.m^{-1}.s^{-1}$), and P is pressure (Pa). A more refined permeability model can incorporate temperature and pressure dependence for better accuracy.

- Effective Specific Heat Capacity:

The effective specific heat capacity, accounting for the contributions from gas and solid phases, is calculated by [42]:

$$(\rho C_P)_{eff} = \varepsilon\rho_g C_{p,g} + (1-\varepsilon)\rho_s C_{p,s} \tag{7}$$

where ε is bed porosity (dimensionless), ρ_g and ρ_s are gas and solid densities ($kg.m^{-3}$), respectively, $C_{p,g}$ and $C_{p,s}$, are the corresponding specific heat capacities ($J.kg^{-1}.K^{-1}$).

- Pulsed (ON-OFF) Heat Load Modeling:

To model a periodic (ON-OFF) heat load system mathematically, we define the heat input Q(t) as a function of time that alternates between an "ON" state, where heat is applied, and an "OFF" state, where no heat is applied. This can be represented using a square wave function, which switches between two levels at specified intervals. One way to express Q(t) is using the Heaviside step function H(t), defined as [43]:

$$H(t) = \begin{cases} 0 \text{ if } t < 0 \\ 1 \text{ if } t \geq 0 \end{cases} \tag{8}$$

For a heat load that turns on at $t = nT$ and OFF at $t = nT + \tau$ for $n = 0, 1, 2, \ldots$ where T is the period and τ is the duration of the "ON" state within each period, the heat input can be modeled as:

$$Q(t) = Q_0\sum_{n=0}^{\infty}[H(t-nT) - H(t-nT-\tau)] \tag{9}$$

This formulation creates a series of pulses, each of duration τ, occurring every T seconds. The difference $H(t-nT) - H(t-nT-\tau)$ represents a pulse that starts at $t = nT$ and ends at $t = nT + \tau$. By incorporating this periodic heat input function into the governing heat

transfer equations, one can analyze the thermal behaviour of systems subjected to cyclic heating, which is essential in applications like material processing, electronic device operation, and thermal management systems. Electrical/control overhead and heater thermal inertia losses were not included in the present model, as the focus was on the intrinsic tank-level thermal performance. These parasitic losses will be addressed in future full-system studies. Beyond numerical performance, it is important to evaluate the practical feasibility of implementing such a pulsed heating strategy in real hydrogen storage systems. In a practical system, ON/OFF heat-flux sequencing could be implemented using programmable power controllers (e.g., solid-state relays or SCR-based modules) linked to temperature and/or pressure feedback from embedded sensors in the vessel wall or hydride bed. The 15-min ON/OFF cycles investigated in this work are significantly longer than the response times of typical control electronics, meaning the required timing precision is well within commercially available capabilities. From a durability standpoint, both MgH_2 and stainless steel have been reported to exhibit stable structural integrity over many thermal cycles within the studied temperature range (300–660 K), although long-term fatigue testing under repeated cycling would be required for commercial deployment. Economically, the pulsed-heating approach does not require additional internal structures such as fins or metal foams, which can reduce hydride volume and increase manufacturing cost. Instead, it relies on relatively low-cost control hardware and external heaters, potentially offering a lower-cost alternative to conventional embedded heat-exchanger designs.

2.3. Assumptions and simplifications

Due to the focus of this study on the temperature dependence of the thermal conductivity during the hydrogen removal process, the following assumptions and simplifications are applied in the numerical analysis:

- **Uniform bed porosity:** The porosity of the magnesium hydride bed is assumed to be uniform and constant during the dehydrogenation process. Variations due to particle size distribution, structural deformation, or local compaction effects are ignored [14].

  Local thermal equilibrium (LTE): LTE between hydrogen and the hydride bed is assumed. Its validity is supported by a separation-of-timescales estimate using packed-bed correlations for interphase heat transfer [44]. For the hydrogen–solid interface in our operating range, the convective heat transfer coefficient is typically $h \approx 300–2000\ W{\cdot}m^{-2}{\cdot}K^{-1}$ [20], while the metal hydride particle diameters are in the range $d_p = 0.1–1$ mm [8]. The characteristic gas–solid thermal equilibration time can be estimated as:

$$\tau_{gs} = \frac{\rho_s c_s d_p}{6h} \tag{10}$$

where ρ_s and c_s are the density and specific heat capacity of the solid particles, respectively.For the above ranges of h and d_p, τ_{gs} falls between 0.02 and 1.4 s, which is two to four orders of magnitude shorter than the ON or OFF pulse durations used in this study (≥ 150 s). Because τ_{gs} is so short, any temperature difference between the solid and gas phases during a heating pulse remains very small, typically $\Delta T_{gs} \approx \tau_{gs} \times (dT/dt)$, which in our conditions corresponds to sub-kelvin offsets. This justifies the use of the Local Thermal Equilibrium (LTE) assumption in our model, as is common in metal-hydride reactor simulations under similar operating conditions. However, we note that under very rapid transients or with much lower h values, a Local Thermal Non-Equilibrium (LTNE) formulation may be necessary [45].

- **Negligible radiative heat transfer:** Radiative heat transfer is eliminated due to its minimal contribution to the overall heat transfer mechanism in the metal hydride structure. The dominant heat transfer processes include conduction and convection [20].
- **Hydrogen as an ideal gas:** Hydrogen is assumed to be an ideal gas, and its thermophysical properties are modeled according to the ideal gas laws. Non-ideal effects such as compressibility or molecular interactions are ignored [17].
- **Constant specific heat capacity:** The specific heat capacity of the solid phase (magnesium hydride) and the gas phase (hydrogen) are assumed to be constant during the entire desorption process, and their variations due to temperature changes are ignored [13].
- **Neglect of structural deformation of the hydride bed:** The volume changes of the metal hydride bed due to phase transformation and hydrogen release are assumed to be negligible. The structural stability of the porous medium remains constant and unchanged during the desorption process [42].
- **Stepwise heat flux representation:** For the stepwise (ON-OFF) heating approach, it is assumed that the changes between heating cycles occur instantaneously and without transfer effects. The thermal inertia effects due to heat flux switching are not explicitly modeled [43].

These assumptions help simplify the numerical analysis and allow us to focus on a detailed investigation of the effects of thermal conductivity's temperature dependence on the hydrogen removal process.

2.4. Boundary conditions and initial conditions

This describes the boundary conditions governing the hydrogen release process in a magnesium hydride (MgH_2) tank subjected to two different external heating methods: constant heat flux and stepwise heat flux (ON-OFF). Fig. 2 shows the boundary conditions for each case, while Table 2 summarizes the corresponding boundary conditions.

The numerical simulation with well-defined initial conditions was validated for the use of adaptation methods in hydrogen utilization modeling. The entire computational domain was initialized at a uniform temperature of 553 K at the start of the simulation. The hydrogen pressure in the metal hydride bed is assumed to be 1.1 bar, which represents the condition before the start of hydrogen consumption. At $t = 0$, the magnesium hydride (MgH_2) bed is fully saturated with hydrogen, meaning that the initial hydrogen volume fraction is assumed to be $x = 1.0$. As the desorption progresses, the hydrogen gas diffuses outward through the porous medium and finally exits the system through the hydrogen outlet at a pressure of 1 bar. In the constant flux mode, heat is continuously and uniformly introduced into the tank through the

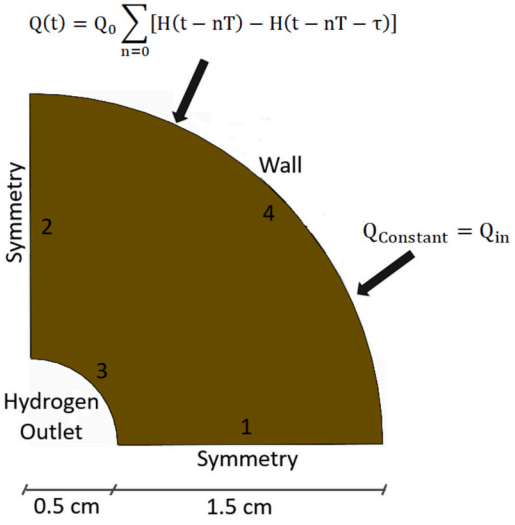

Fig. 2. Geometry and the definition of boundary conditions.

Table 2
Boundary values for each boundary.

Boundary Conditions	Location	Value/Description
Hydrogen Outlet Pressure	Boundary 3	$P = 1$ bar
Thermal Insulation	Boundaries 1–3	$\nabla \cdot q = 0$ (no heat flux)
Constant Heat Flux	Boundary 4	$q = q_{in} = 6700\ W/m^2$
Stepwise Heat Flux	Boundaries 4	$Q(t) = Q_0 \sum_{n=0}^{\infty} [H(t - nT) - H(t - nT - \tau)]$
Symmetry	Boundaries 1,2	

external steel boundary, causing a uniform increase in the hydride bed. In the stepwise flux mode, heat is alternately turned ON and OFF, which contributes to the heat diffusion mode, temperature uniformity, and the reduction of hot spots. These boundary and initial conditions provide a comprehensive environment for the thermal analysis of hydrogen performance under different heating strategies and can systematically represent these two physical temperatures in the process of hydrogen release from the magnesium hydride bed.

2.5. Numerical simulation workflow

A structured numerical workflow was developed and implemented in this study to evaluate the thermal efficiency and hydrogen desorption performance under two different heat flux strategies: constant and stepwise (ON/OFF) heat application. The main objective of this evaluation is to identify the optimal heat transfer method that minimizes the hydrogen desorption time in magnesium hydride (MgH_2), which has a direct impact on the effectiveness of the system in real-world hydrogen delivery applications. The comparative framework is organized as two independent and parallel simulation channels, each of which investigates one of the thermal management strategies.

As far as can be seen in Fig. 3, in the first channel, a constant heat flux is continuously applied to the external boundary of the magnesium hydride tank. The hydrogen desorption time is recorded, and this value is taken as the baseline performance against which other strategies will be compared. The second channel focuses on the stepwise heat flux

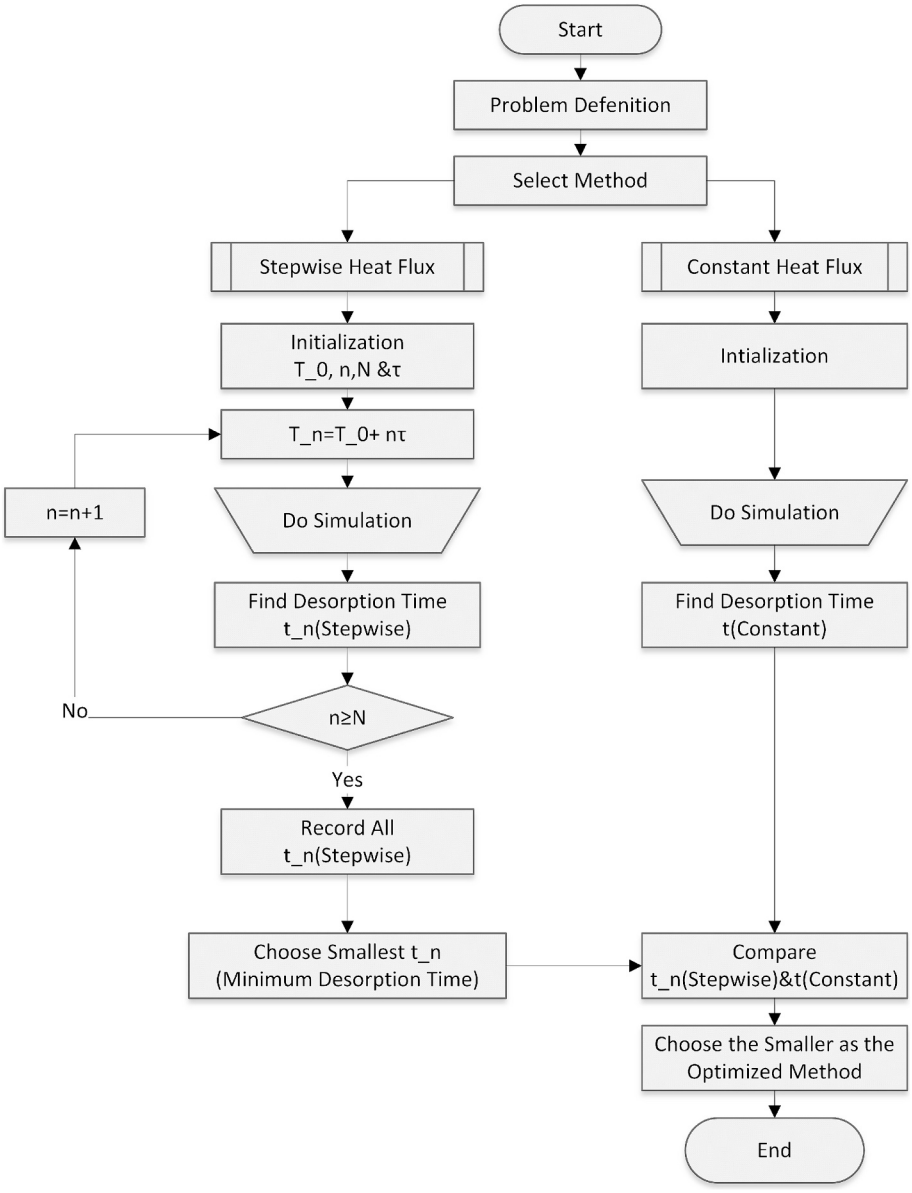

Fig. 3. Methodology of the numerical simulation.

approach, in which heat is applied periodically in an ON/OFF pattern over time. Since there is no predefined optimal interval for the switching frequency of the stepwise method, an internal optimization process is employed. The optimization process begins by selecting an initial time interval, 1 min ON followed by 1 min OFF, and a full simulation is performed to determine the corresponding desorption time. The time interval is then repeatedly adjusted by a defined increment, a new ON/OFF pattern is created for each step, and the desorption time for each interval is recorded and added to the growing dataset. Once the optimal interval is identified in the stepwise method, this value is directly compared to the desorption time obtained from the constant heat flux simulation. The objective function of this optimization is to minimize the total hydrogen desorption time. Therefore, the ON/OFF cycle that results in the quickest 99 % hydrogen release is selected as the optimal configuration. This provides a quantitative basis for comparing the two strategies. This comparative analysis, focusing on the hydrogen desorption time as a key performance indicator, provides a practical basis for selecting an optimal thermal management strategy that improves both energy efficiency and desorption kinetics.

2.6. Mesh Independence analysis

To ensure the reliability and numerical stability of the simulation results, an independent mesh study was conducted using five different mesh densities ranging from coarse to highly refined settings. The objective of this evaluation was to investigate the effect of mesh resolution on two important output parameters, namely Darcy's velocity magnitude and average temperature during the hydrogen desorption process in a magnesium hydride (MgH_2) tank.

The mesh structure was designed using a mapped quadrilateral scheme, which was chosen due to its compatibility with the symmetric geometry of the domain and its ability to maintain geometric compliance and increase computational efficiency. Five distinct mesh densities including 144, 240, 484, 1520, and 6004 elements were implemented and tested under identical boundary and initial conditions, and for each case, simulations were performed and the resulting equilibrium pressure and peak temperature were recorded, as summarized in Fig. 4. The results showed that mesh refinement beyond 1520 elements produced negligible changes in darcy's velocity magnitude and average bed temperature. In particular, the difference between the fourth and fifth mesh configurations was minimal. The average temperature changed by only 0.17 K, representing a 0.73 % variation, and the magnitude of Darcy's velocity showed a difference of just 1.07 %, indicating that the solution was nearing numerical convergence with the optimized mesh size. These findings indicated that the fourth mesh configuration, consisting of 1520 elements, strikes a good balance between numerical accuracy and computational efficiency. To confirm the reliability of the model, a validation was also performed against experimental data from Chaise et al. [46] and Lutz et al. [20], as described in Section 3.1, showing excellent agreement in both temperature profiles and hydrogen desorption trends.

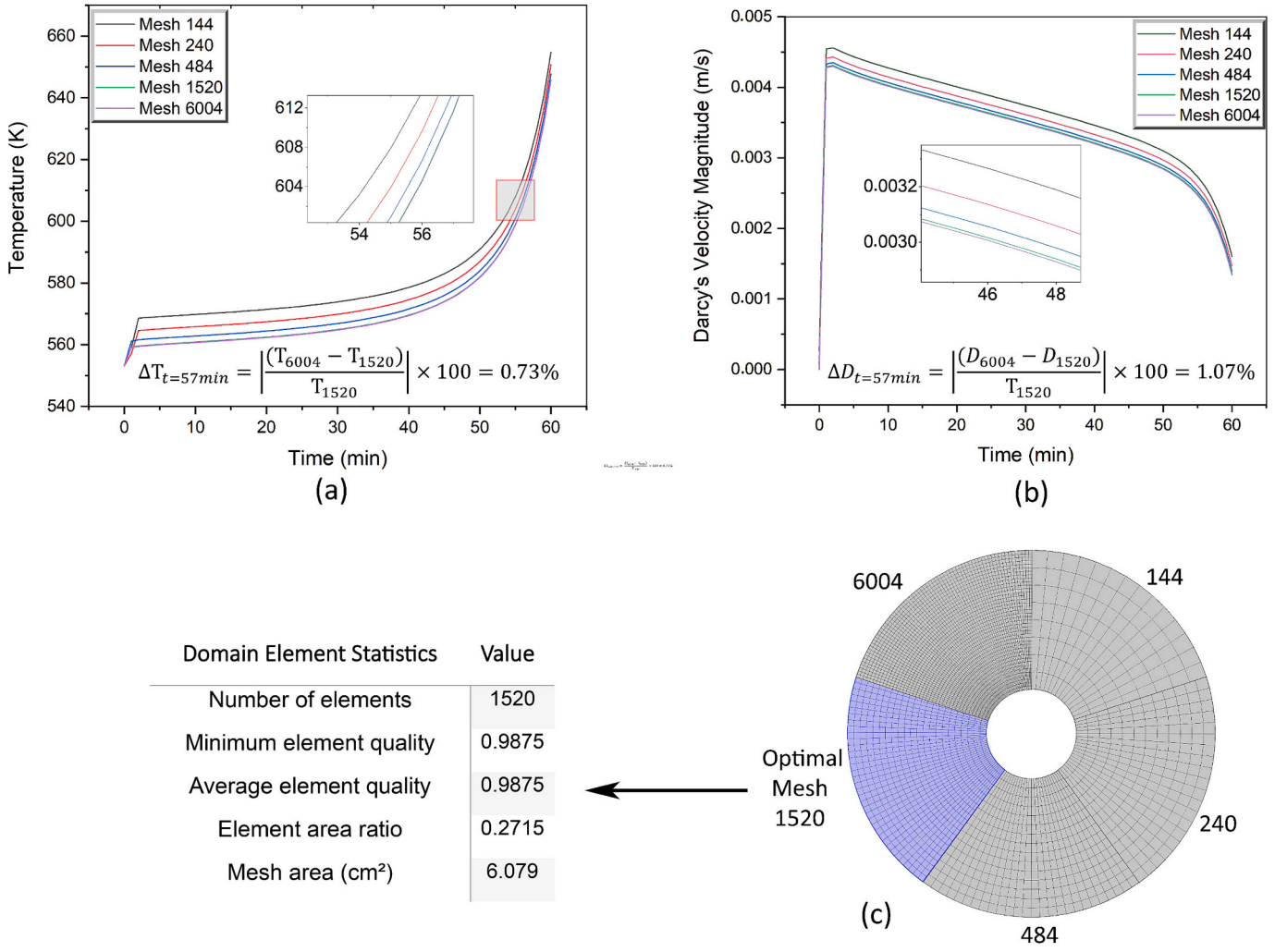

Fig. 4. Mesh independence analysis based on temperature and Darcy's velocity magnitude.

3. Results and discussion

3.1. Validation

To ensure the validity and accuracy of the numerical results presented in this study, the simulation outputs were validated against experimental and numerical benchmark data presented by Chaise et al. [46]. Their experimental dataset is one of the most comprehensive investigations of magnesium hydride systems, accurately recording the temperature evolution and hydrogen desorption behaviour in the temperature range of 550–650 K under a hydrogen pressure of approximately 1 bar. In parallel, the numerical data reported by Chaise et al. [46] and Lutz et al. [20] also serve as a valuable benchmark to validate the performance of the present model under similar boundary and operating conditions, and provide a strong framework for evaluating the thermal behaviour and hydrogen desorption volume predicted by the current numerical simulations.

Fig. 5(a) shows the comparative temperature profiles between experimental observations, the numerical model of Chaise et al. [46] and Lutz et al. [20], and the current simulation, which shows a high degree of agreement, especially in the first 400 min of the desorption process. The average temperature deviation remained between 0.2 and 0.4 K at most time steps, corresponding to a relative error of less than 1 %. Since the main focus of this study is the comparison between constant and stepwise heat flux strategies, this validation supports the model's ability to reliably evaluate and differentiate the performance of each method, especially in predicting the desorption time and temperature evolution during the desorption process.

Furthermore, the validation was extended to the analysis of the volume of hydrogen desorbed over time, which is a critical performance indicator for assessing the effectiveness of the hydrogen release process. As shown in Fig. 5(b), the simulation results closely follow the experimental trends, especially in the early and mid-stage hydrogen release intervals (0–450 min), and the model successfully captures the nonlinear kinetics of hydrogen release that occurs as a result of temperature gradients and equilibrium pressure drop in the hydride structure. Although slight deviations are observed in the later stages, they can be attributed to differences in the experimental setup, such as boundary layer effects and latent heat exchange at the reactor wall, which are often difficult to replicate exactly in numerical simulations. Overall, the close alignment between the current simulation outputs and the reference experimental and numerical data sets confirms the robustness of the proposed model, and the results show that the applied boundary conditions and kinetic equations effectively replicate the physical behaviour of hydrogen desorption from magnesium hydride tanks.

3.2. Analysis of desorption process by application of constant heat flux

Fig. 6 illustrates the time evolution of the hydrogen desorption kinetics of magnesium hydride along with the corresponding temperature distribution within the metal hydride bed under constant heat flux conditions. The data are shown at five distinct time intervals, 0, 15, 30, 45, and 60 min, capturing the full progression of the desorption process. At the initial stage ($t = 0$), the magnesium hydride tank is completely saturated with hydrogen, and no desorption or thermal diffusion is observed. By 15 min, a narrow active zone forms near the heat source, corresponding to a moderate rise in temperature. The initial contour plots indicate that the desorption process begins gradually and propagates radially inward, driven by thermal diffusion. However, due to the inherently low thermal conductivity of magnesium hydride, the transfer of heat towards the core is considerably delayed, resulting in the formation of a steep radial temperature gradient.

This phenomenon becomes more pronounced over time. At $t = 30$ and 45 min, the reaction zone expands, yet the temperature difference between the hot outer boundary and the cooler central region increases progressively. The limited thermal conductivity prevents uniform heat distribution, delaying the activation of the desorption process in the central parts of the bed. By the final stage ($t = 60$ min), the system temperature exceeds 653 K, and the temperature difference across the domain reaches approximately 14 K. The temperature contours reveal a sharp increase in gradient, confirming that the outer regions undergo lower thermal gain compared to the core, where the unreacted hydride has begun to decompose rapidly. In parallel, the hydrogen desorption kinetics exhibit a continuous and gradually accelerating trend. During the early and intermediate stages of the process, the applied thermal energy is primarily absorbed by the endothermic desorption reaction, resulting in a relatively stable and moderate temperature increase. However, as the reaction approaches completion, particularly between 45 and 60 min, the concentration of hydrogen within the tank decreases substantially. Consequently, less heat is consumed by the reaction, and

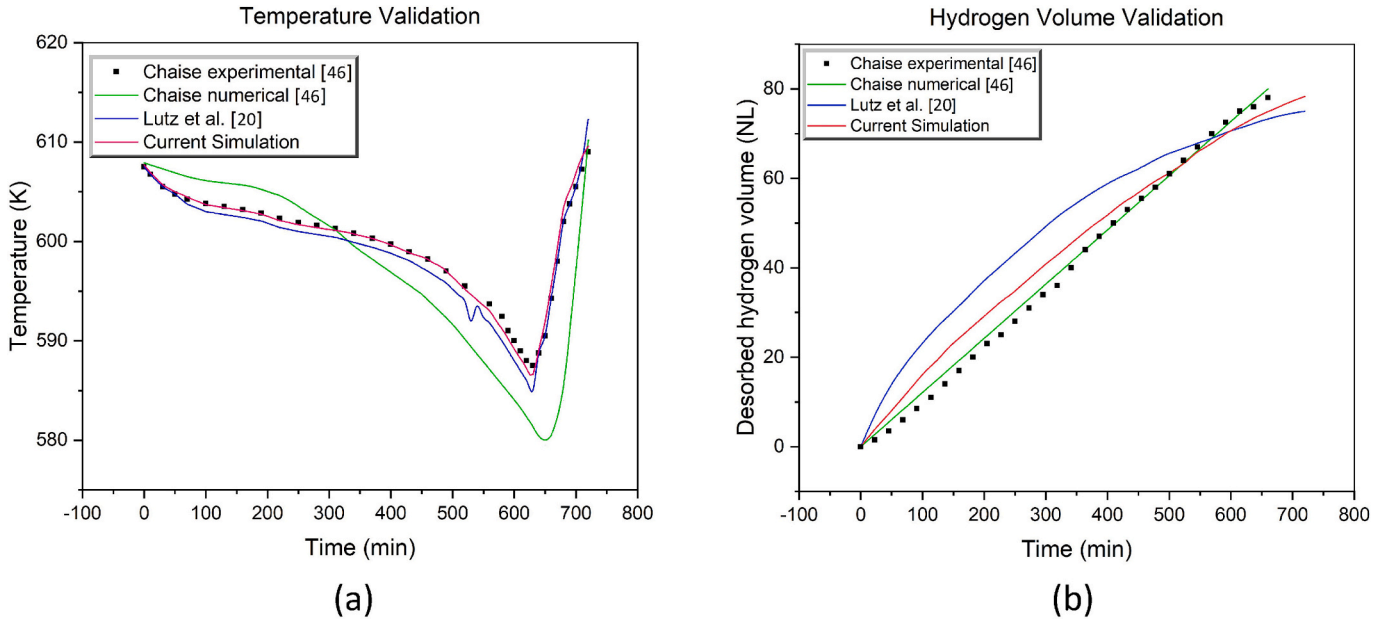

Fig. 5. Validation of the present numerical model against experimental and numerical benchmarks.

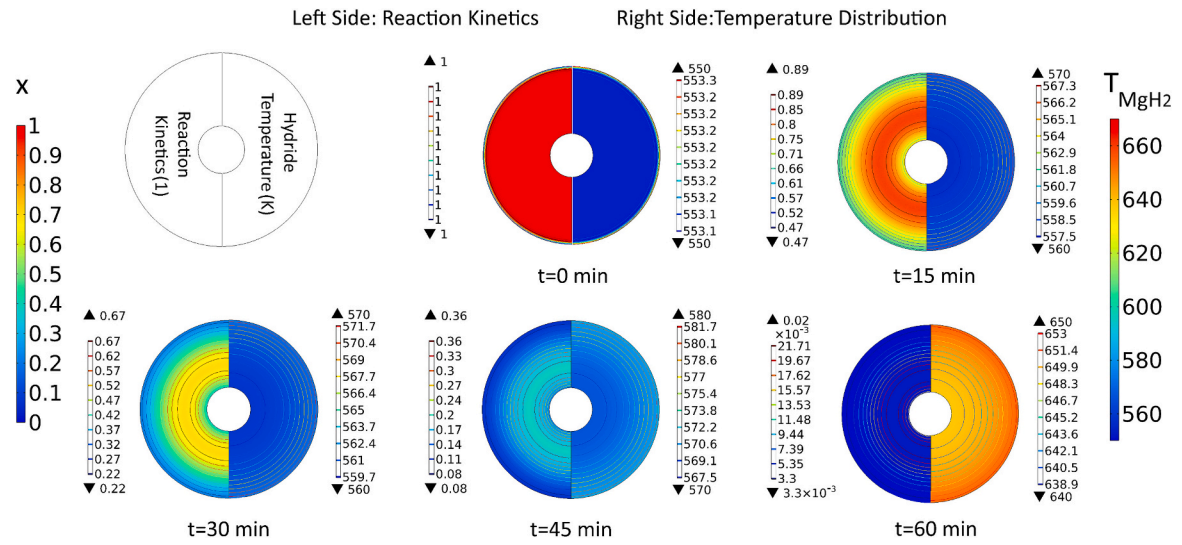

Fig. 6. Temperature and reaction kinetics contours under constant heat flux.

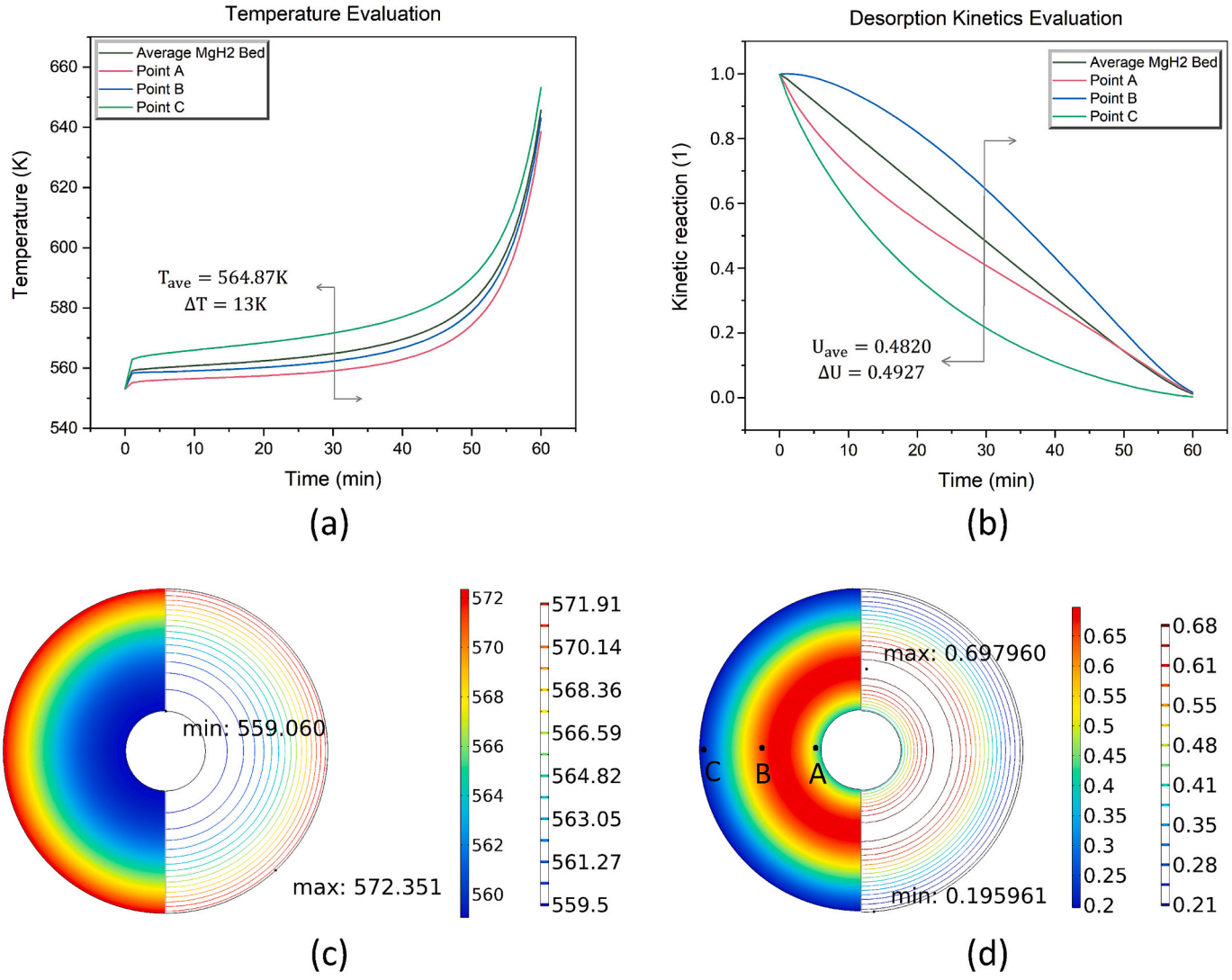

Fig. 7. Temperature and reaction kinetics contours at selected points in the MgH_2 bed under constant heat flux.

the remaining energy begins to accumulate in the solid structure, leading to a noticeable increase in local temperature. This effect is evident as a thermal jump of approximately 72 K during this final phase. Once the endothermic demand is reduced due to hydrogen depletion, the incoming heat is no longer absorbed as effectively, causing a rapid temperature rise, a phenomenon that often causes hot spot generation in the bed structure. The low thermal conductivity not only causes uneven temperature fields but also constrains the rate and spatial extent of the hydrogen release process. The combined analysis of temperature and reaction contours (Fig. 7) reveals that under constant heat flux, the system develops notable temperature gradients and localized desorption zones, underscoring the need for improved thermal management to ensure uniform hydrogen release and efficient energy use throughout the tank.

Temperature and kinetic behaviors were analyzed at three key points in the MgH_2 bed: point A (near the outlet), point B (mid-radius), and point C (near the heat source), as shown in the 2D contours (Fig. 7d). Over the 60-min process shown in Fig. 7(a), temperature rises across all areas, but the increase varies spatially. Point C exhibits the highest temperature, while point A shows the lowest. At 30 min, a temperature difference of $\Delta T = 13$ K is observed between these two regions, despite an average bed temperature of 564.87 K. This inhomogeneity, confirmed by the temperature contour in Fig. 7(c), reflects the low thermal conductivity of the hydride, as temperature drops from 572.14 K to 559.13 K. Reaction kinetics analysis in Fig. 7(b) shows point C reaching full desorption fastest due to its elevated temperature. Surprisingly, the lowest reaction rate appears at point B (0.1996 $m.s^{-1}$), not at the cooler point A. At 30 min, a kinetic difference of $\Delta U = 0.4927$ $m.s^{-1}$ is noted across the tank. The reduced desorption rate at point B, despite moderate temperature, suggests transport resistance and local pressure drop in the porous structure hinders gas evacuation. This is evident in the kinetic contour of MgH_2 in Fig. 7(d), where desorption lags in the central region. It is evident from the results that the desorption rate depends not solely on temperature but also on hydrogen transport dynamics, pressure gradients, and bed structure. This behaviour aligns with previous studies and reinforces the importance of incorporating models such as Darcy's law and ideal gas assumptions to capture the complex, coupled behaviour within the hydride reservoir.

3.3. Impact of thermal conductance on desorption time

Based on the results of numerical analyses and observations presented in the previous sections, it was found that one of the key factors in creating temperature gradients and fluctuations in hydrogen desorption rate in metal hydride beds is the limitation in the thermal conductivity of MgH_2. To investigate this issue more precisely, in this section, the effect of changing thermal conductivity in the range of 1 to 10 $W{\cdot}m^{-1}{\cdot}K^{-1}$ on the temperature profile and kinetics of the desorption reaction is investigated. The conductivity intervals reported in Table 3 follow experimentally observed performance thresholds from prior studies, particularly those by Lutz et al. [20] and Chaise et al. [46], which were also used for model validation. In these works, $\lambda = 4.2$ $W{\cdot}m^{-1}{\cdot}K^{-1}$ was identified as an optimal effective conductivity for MgH_2 composites with expanded graphite; values above this level produced negligible further improvement in desorption performance. The lower bands (1–2.5 and 2.5–4.2 $W{\cdot}m^{-1}{\cdot}K^{-1}$) correspond to moderate enhancement achievable via small additive fractions or partial contact improvements, while the upper bands (4.2–7.5 and 7.5–10 $W{\cdot}m^{-1}{\cdot}K^{-1}$) represent stronger enhancement from higher additive content or improved particle alignment. This classification ensures meaningful performance comparison while reflecting realistic, literature-supported conductivity ranges.

Fig. 8 shows that as thermal conductivity increases, the reaction kinetics accelerate, leading to faster hydrogen desorption and earlier evacuation of the tank. At the same time, the average temperature across the bed decreases due to improved heat distribution. This improvement in thermal distribution leads to a more uniform desorption reaction throughout the tank, especially in the middle regions and far from the heat source, regions where the reaction occurred with a delay in the initial conditions. However, beyond a certain value (4.2 $W{\cdot}m^{-1}{\cdot}K^{-1}$, which is also known as the experimentally reported value [46]), further increases in thermal conductivity do not show a significant effect on the improvement of the desorption process. Table 3 summarizes the percentage change in bed temperature and reaction kinetics between successive thermal conductivity values measured at $t = 57$ min. This time point corresponds to approximately 95 % desorption.

As shown, increasing λ from 1 to 2.5 $W{\cdot}m^{-1}{\cdot}K^{-1}$ results in the most significant changes, with a temperature drop of 2.78 % and a reaction difference of 13.48 %. The improvement becomes more modest from 2.5 to 4.2 $W{\cdot}m^{-1}{\cdot}K^{-1}$, where ΔT decreases to 0.51 % and Δx to 2.10 %. Beyond 4.2 $W{\cdot}m^{-1}{\cdot}K^{-1}$, the enhancements taper off significantly, between 4.2 and 7.5 $W{\cdot}m^{-1}{\cdot}K^{-1}$, ΔT is only 0.06 % and Δx just 0.97 %, and from 7.5 to 10 $W{\cdot}m^{-1}{\cdot}K^{-1}$, the changes drop further to 0.02 % and 0.23 %, respectively. These results confirm that $\lambda = 4.2$ $W{\cdot}m^{-1}{\cdot}K^{-1}$ is the optimal value, as further increases yield diminishing returns in both temperature uniformity and reaction enhancement.

3.4. Evaluation of MgH_2 reaction under different step heating periods

In this section, the effects of four different ON/OFF step heating

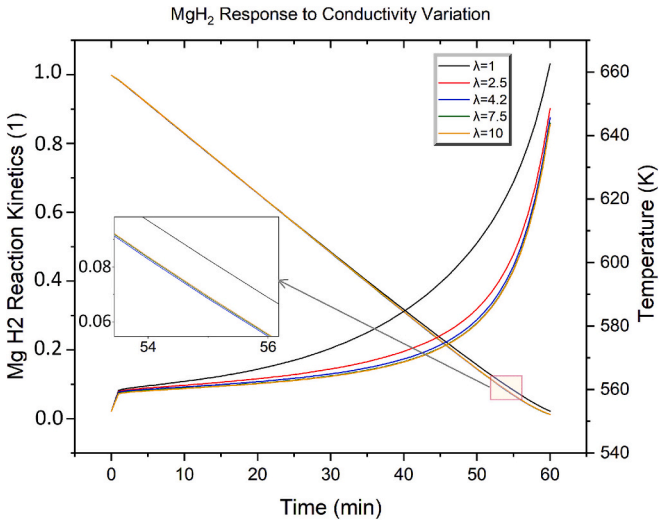

Fig. 8. Effect of varying thermal conductivity on temperature distribution and desorption kinetics in the MgH_2 bed.

Table 3
Percentage differences in temperature and reaction kinetics for successive thermal conductivity values.

Conductivity Pair ($W{\cdot}m^{-1}{\cdot}K^{-1}$)	T_i (K)	T_{i+1} (K)	$\Delta T = \left\lvert\frac{(T_{i+1}-T_i)}{T_i}\right\rvert \times 100$	x_i (1)	x_{i+1} (1)	$\Delta x = \left\lvert\frac{(x_{i+1}-x_i)}{x_i}\right\rvert \times 100$
1 → 2.5	650.51	632.44	2.78 %	0.066	0.0571	13.48 %
2.5 → 4.2	632.44	629.23	0.51 %	0.0571	0.0559	2.10 %
4.2 → 7.5	629.23	628.82	0.06 %	0.0559	0.0554	0.97 %
7.5 → 10	628.82	628.7	0.02 %	0.0554	0.053	0.23 %

periods (2.5, 5, 10, and 15 min) on two key parameters in the MgH_2 system are investigated: MgH_2 reaction kinetics and temperature distribution. The main objective of the analysis is to identify the most efficient thermal pulse duration that optimizes both thermal efficiency and overall system performance. Fig. 9a illustrates the changes in reaction kinetics over time for each heating duration. In the $\Delta\tau = 2.5$ min cycle, the reduction in desorption kinetics occurs gradually and slowly, indicating insufficient heat penetration into the hydride bed. In the $\Delta\tau = 5$ min case, kinetic performance is slightly improved, though it still follows a uniform and moderate declining trend. Increasing the heating duration to $\Delta\tau = 10$ min leads to a noticeable acceleration in the reaction rate, particularly in the mid-to-late stages of the process, reflecting improved heat transfer into the inner regions of the bed. Finally, the $\Delta\tau = 15$ min cycle exhibits the highest and most stable reaction rate, resulting in the most efficient hydrogen desorption.

Fig. 9b presents the corresponding temperature variations for each heating case. In the shorter cycles (e.g., 2.5 min and D-D′ points), although temperature initially increases, the frequent OFF periods cause significant fluctuations and prevent consistent thermal buildup. The 5-min cycle yields a more stable temperature rise, but the peak temperature remains insufficient for rapid desorption. In contrast, the 10-min cycle shows a more continuous and elevated temperature increase, especially in the second half of the process. In the optimal 15-min cycle, the temperature exceeds 661.4 K (point A') with minimal fluctuation, indicating more effective and uniform heat accumulation and distribution throughout the hydride bed. The combined thermal and kinetic evaluation demonstrates that longer ON durations improve thermal stability and complete activation of the desorption front within the porous hydride structure. Among the tested configurations, the 15-min stepwise heating cycle (point A) is identified as the optimal mode, providing superior temperature control and the highest hydrogen release efficiency. The superior performance of the 15-min cycle is consistent with TCEF: longer ON intervals generate more Mg per pulse, raising the bed's thermal conductivity and enabling subsequent pulses to heat the material more effectively. In other words, each extended heating phase creates a larger jump in conductivity, which self-reinforces the desorption front in following pulses. This configuration will be used as the reference case in the next section for comparison with the conventional constant heat flux heating method. Quantitative confirmation is provided in Table 4. Desorption time, defined at 99 % hydrogen release, falls monotonically from 60 min (constant flux) to 45 min ($\Delta\tau = 15$ min). Average bed temperature rises correspondingly, while peak temperature remains well below the design limit of 661 K in every case.

Table 4
Boundary values for each boundary.

Metric	Constant Heat Flux	2.5 min ON/OFF	5 min ON/OFF	10 min ON/OFF	15 min ON/OFF
Desorption Time (to 99 % H_2 release) (min)	60	58	55	50	45
Average Bed Temperature (K)	645.58	649.76	660.2	660.91	661.05
Maximum Bed Temperature (K)	653.77	661.07	677.71	677.9	677.98
Average Equilibrium Pressure (Pa)	1.04×10^6	1.13×10^6	1.45×10^6	1.46×10^6	1.46×10^6
Maximum Equilibrium Pressure (Pa)	1.23×10^6	1.43×10^6	2.015×10^6	2.016×10^6	2.017×10^6
Average Darcy Velocity (m/s)	0.00135	0.0016	0.0021	0.00277	0.00294
Maximum Darcy Velocity (m/s)	0.01728	0.0342	0.0345	0.03452	0.03453
Maximum Temperature Gradient (K/m)	1276.43	3145.67	3160.5	3193.14	3205.17
Sensible Heat Stored at End (kJ/m^3)	0	0.463	1.27	2.3	3.4
Energy Efficiency (qualitative)	Very Low	Low	Moderate	High	Highest

Although pulsed heating inevitably produces higher instantaneous pressures and velocities, the 15-min cycle secures the most favorable averages (equilibrium pressure = 1.46×10^6 Pa and Darcy's velocity = 2.94×10^{-3} $m.s^{-1}$, respectively) without compromising stability. Most importantly, the recoverable sensible-heat reservoir grows from 0 $kJ.m^{-3}$ under constant flux to 3.4 $kJ.m^{-3}$ under the 15-min cycle, demonstrating a clear energy-saving benefit. The qualitative energy-efficiency ranking in Table 4 therefore progresses logically—Very Low

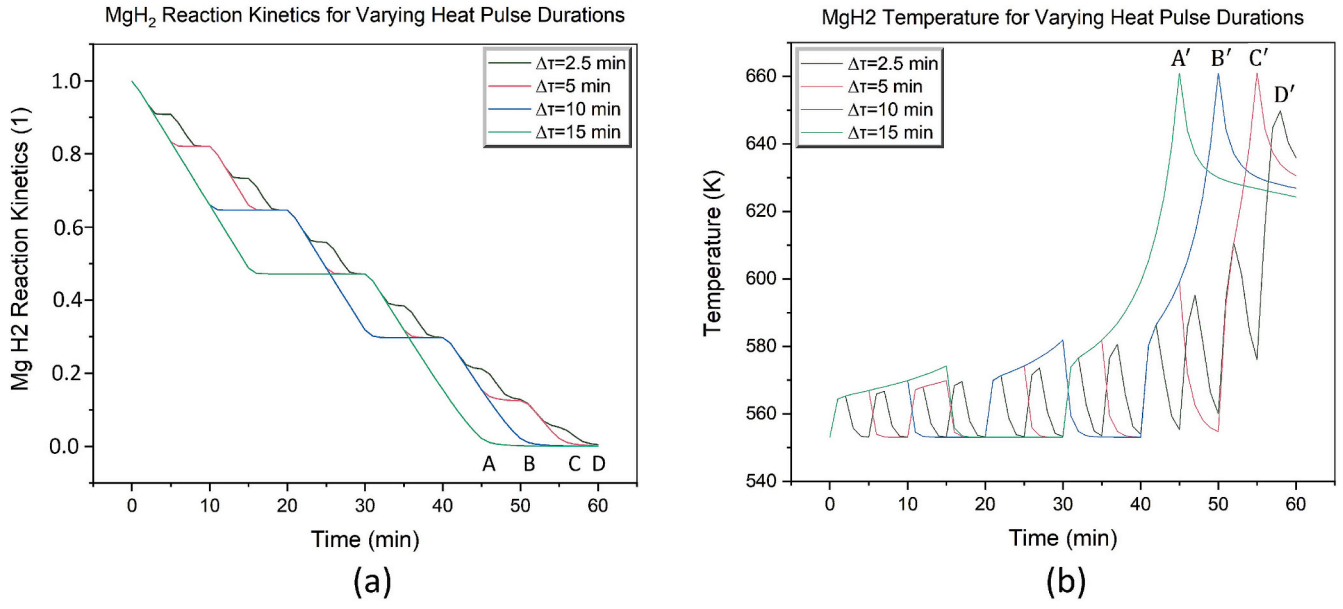

Fig. 9. Effect of different stepwise heating durations on (a) MgH_2 reaction kinetics and (b) temperature distribution.

→ Highest—as pulse duration increases. Taken together, Fig. 9 and Table 4 show a coherent progression:

1. Thermal-penetration phase ($\Delta\tau \leq 5$ min). Heat input is too brief; temperature oscillations dominate, and reaction stalls.
2. Transition phase ($\Delta\tau = 10$ min). Each pulse is long enough to raise the wall well above equilibrium temperature, driving faster desorption, yet it still incurs noticeable thermal cycling losses.
3. Optimized phase ($\Delta\tau = 15$ min). Wall temperature climbs smoothly, radial gradients flatten, and hydrogen is released 25 % faster than under constant heating while saving external energy and storing a useful sensible-heat buffer.

Longer symmetric pulses would converge towards steady heating with no further kinetic gain, whereas shorter pulses underutilize the heater. The 15 min ON/OFF sequence is therefore adopted as the optimized heat-flux schedule for the remainder of this study. Future work will relax the 50 % duty-cycle constraint—e.g., testing 20 min ON / 10 min OFF, to determine whether asymmetric schemes can deliver additional marginal improvements. Although Eq. 9 idealizes the wall heat flux as an instantaneous square wave, in practice, heaters have finite thermal response times due to their thermal mass. This behaviour can be represented by a first-order lag with a characteristic heater time constant τ_h, which is the time required for the heat flux to reach about 63 % of its steady-state value after a sudden change in power input. The formula of the heater's output during the ON period can be expressed as Eq.11 [47]:

$$q''_{on} = q''_0\left[1 - \frac{\tau_h}{t_{on}}\left(1 - e^{-t_{on}/\tau_h}\right)\right] \tag{11}$$

So the percentage reduction of shortfall in average ON-segment flux (vs. an ideal square wave) is:

$$R_s = 100 \times \frac{\tau_h}{t_{on}}\left(1 - e^{-t_{on}/\tau_h}\right) \tag{12}$$

where R_s is the reduction of shortfall, t_{on} is the pulse duration in Eq.12. For $t_{on} \gg \tau_h$, the reduction in average flux is small, but for shorter pulses, inertia slightly lowers the effective heating. Table 5 quantifies this reduction percentage for the ON durations in this study and typical τ_h values for compact electric heaters [48].

These results indicate that for the longer ON durations (≥10 min) that yield the best desorption performance in this section, heater inertia would reduce average flux by less than 2 %, which is unlikely to affect the reported trends. Shorter cycles are more sensitive but still within a few percent for τ_h values typical of compact electrical heaters. Including the effect of thermal inertia in future models would enable more detailed optimization of pulse durations and control strategies.

3.5. Assessment of constant versus stepwise heat flux

To investigate the effect of different thermal strategies on the magnesium hydride desorption behaviour, two heat flux application methods, constant flux and stepwise (pulsed) heating, were used over 60 min. Fig. 10(a) shows the heat input profiles for both strategies; in the constant flux method, a uniform value of about 6700 W.m^{-2} is maintained throughout the entire simulation, while the stepwise method uses alternating ON/OFF heat pulses ranging from 0 to 13,400 W.m^{-2} at 15-min intervals. This difference in thermal pattern has a direct and significant impact on the thermal and kinetic response of the metal hydride system, which can be seen in the temperature and reaction rate profiles (Fig. 10 (b)). In the constant heat flux mode, the bed temperature gradually and continuously increased from the initial value of 553.15 K to 645.58 K. This thermal process was accompanied by a uniform and continuous decrease in the reaction fraction from 0.998 to 0.0019, indicating a slow but steady and non-stop hydrogen desorption process. The uniform heat input caused the formation of a regular thermal diffusion in the bed and resulted in a predictable and uniform reaction behaviour.

Table 5
Percentage reduction in average ON-segment wall heat flux.

τ_h (s)	2.5 min (150 s)	5 min (300 s)	10 min (600 s)	15 min (900 s)
2	1.33 %	0.67 %	0.33 %	0.22 %
5	3.33 %	1.67 %	0.83 %	0.56 %
10	6.67 %	3.33 %	1.67 %	1.11 %

On the other hand, in the stepwise method, the system was subjected to discrete thermal cycles. In the first phase (0 to 15 min), the temperature increased rapidly to 574.26 K, leading to a decrease in the reaction fraction from 0.998 to 0.48788. Upon entering the OFF phase (15 to 30 min), the heat input was stopped, and the temperature returned to around the initial value (553.15 K). With the onset of the second ON phase (30–45 min), the temperature increased steeply, reaching a peak of 661.04 K. This re-thermal shock resulted in a significant acceleration of the reaction, such that the reaction fraction at the end of the process reached 0.001, a value slightly lower than in the constant flux case. This dramatic acceleration suggests a TCEF effect: the first ON-phase produces significant Mg (higher λ), so by the second ON-phase heat spreads more rapidly through the now more conductive bed, yielding the observed 're-thermal shock'. Each pulse thus builds on the conductivity gains of the previous cycle, creating a self-reinforcing heating/desorption cycle. The cyclic heating in the stepwise method resulted in nonlinear and oscillatory behaviour in both temperature and reaction parameters. While the OFF periods temporarily halted the desorption process, the ON pulses created a strong thermal gradient and significantly increased the reaction rate in the active phases. From a performance perspective, the stepwise strategy has been shown to maximize the thermal response and accelerate the desorption process. However, periodic interruptions due to quiescent phases can cause local kinetic stagnation and thermal inhomogeneities in some of the beds. Conversely, the constant heat flux approach, by providing continuous and gradual heating, ensures a more stable and controllable desorption, although the initial reaction rate is lower in this case. To complement the time profiles in Fig. 10, Fig. 11 presents five snapshots ($t = 0$, 15, 30, 45, and 60 min) of the bed's spatial distribution, where each image depicts a full circle vertically divided into two semicircles: the left showing reaction kinetics (x) and the right displaying temperature contours. The top row of the Fig. 11 shows the constant heat flux scheme, and the bottom row shows the stepwise strategy (15 min ON / 15 min OFF). At the initial time (t = 0 min), both strategies start from the same conditions: the kinetic semicircles are completely red (x = 1, no reaction), and the temperature semicircles are uniformly blue (553 K), indicating the cold initial conditions.

In the constant heat flux strategy, the temperature field gradually warms up, and a uniform reaction front forms towards the centre of the bed. At $t = 60$ min, the outer surface temperature reaches about 653 K, and the value of x at the surface boundary decreases to about 0.003, indicating continuous, symmetric, and stable hydrogen desorption. In contrast, the stepwise heat flux strategy produces more pronounced thermal pulses and reaction progress. In the ON phases ($t = 15$ and 45 min), the temperature of the right semicircle increases to about 587.3 K and 676.3 K, respectively, and the left semicircles show rapid local release near the surface ($x \approx 0.2$ and $x \approx 0.004$). In the OFF phases ($t =$ 30 and 60 min), the temperature decreases (to about 566 K and 624 K) and the reaction kinetics stops, although the conversion already carried out is maintained. This pattern results in an oscillatory temperature and reaction behaviour with rapid thermal pulses and cooler, stationary intervals. Overall, the constant heat flux strategy provides a smooth, uniform, and predictable kinetic and thermal evolution that is desirable for stable desorption processes. The stepwise approach with intermittent pulses results in more intense heating and reaction acceleration in the active phases, but at the cost of temporal and spatial fluctuations in the

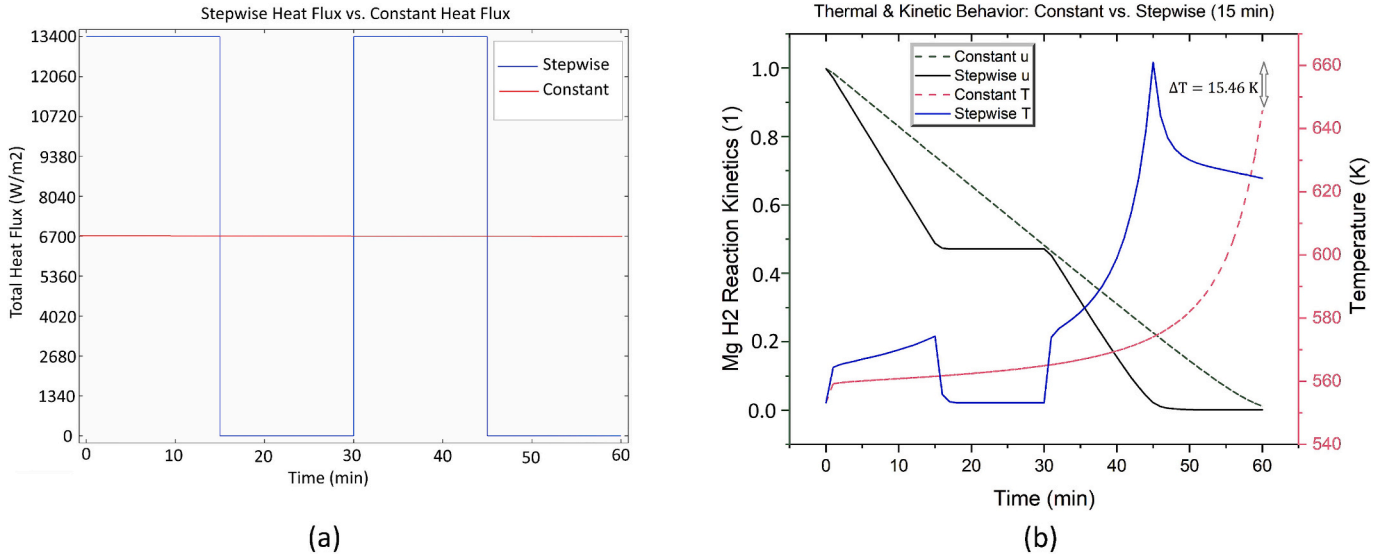

Fig. 10. Comparison of constant and stepwise heat flux strategies on temperature evolution and hydrogen desorption.

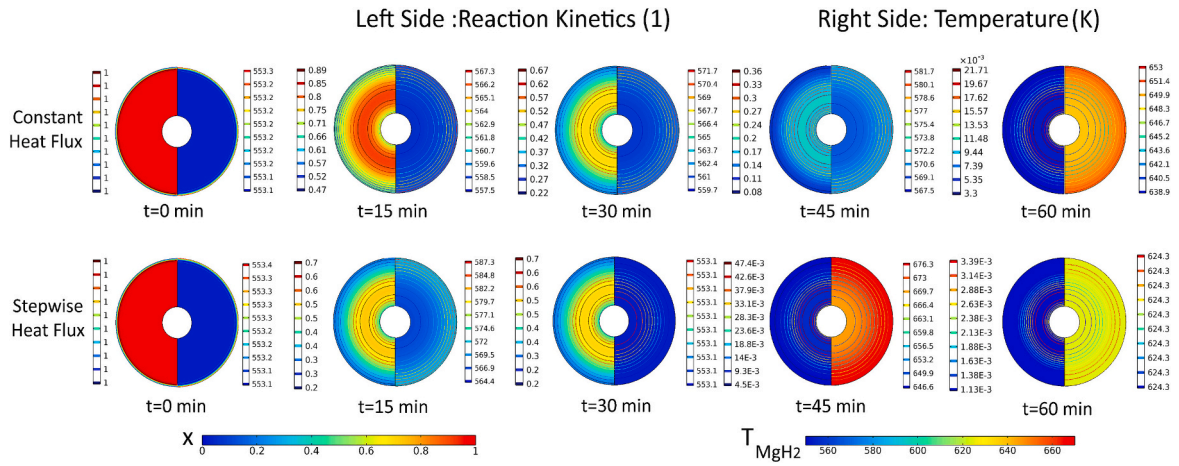

Fig. 11. Thermal and reaction kinetics contours under constant and stepwise heat flux strategies at selected time intervals.

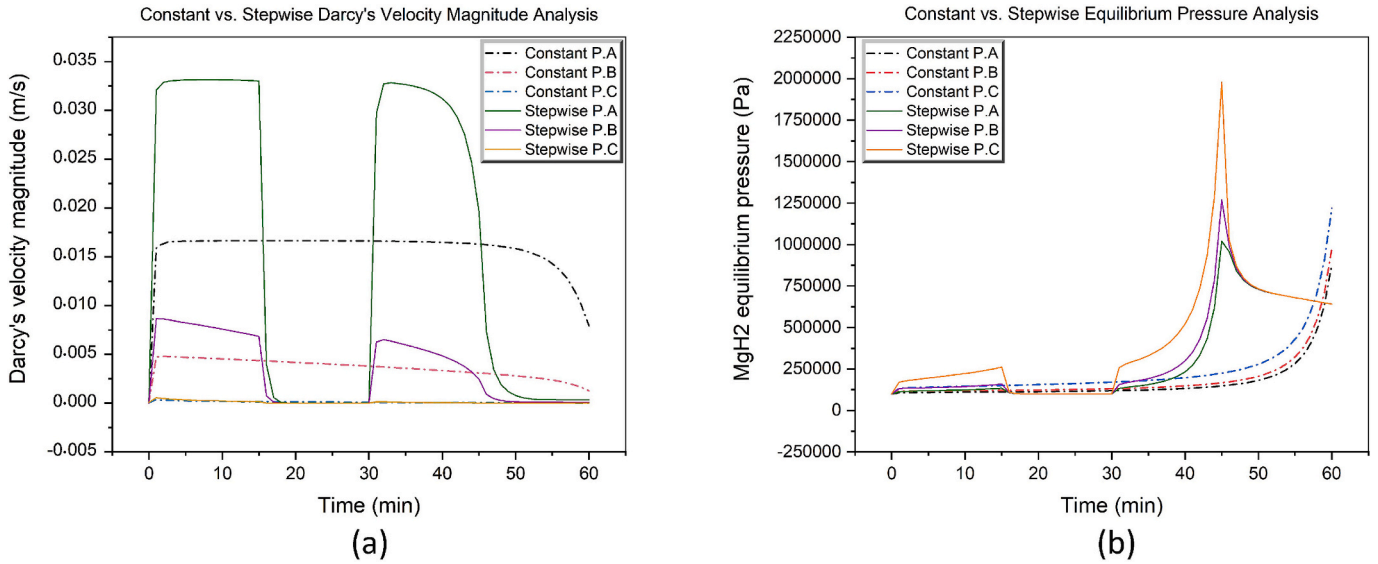

Fig. 12. Evolution of equilibrium pressure at selected radial positions under constant and stepwise heat flux strategies.

thermo-kinetic behaviour of the system.

3.6. Hydrogen flow and pressure response

Fig. 12a and b provide a comprehensive comparison of the magnesium hydride bed's thermal and dynamic performance at three different radial positions: points A, B, and C. This evaluation is performed for two thermal management strategies: constant radial heat flux and stepwise heat flux (ON/OFF cycles). In Fig. 12a, the equilibrium pressure variations over time are shown. Under constant heat flux, the pressure at all three points increases uniformly and continuously, in line with the gradual increase in bed temperature. At the end of the 60-min process, the pressure at point C reaches a peak value of 1.2198×10^6 Pa, while the corresponding values for points B and A are 972,910 Pa and 879,390 Pa, respectively. These pressure differences reflect a stable radial thermal gradient across the bed.

On the other hand, under the stepwise heat flux strategy, the pressure exhibits a periodic oscillation, rising sharply during the heating phases and dropping rapidly during the OFF phases. In this case, the pressure at point C reaches a peak value of 1.9793×10^6 Pa in the second heating cycle, which is the highest value among all points. Points A and B also show a similar oscillatory behaviour, but with lower peak values and a longer time delay, due to their radial distance from the heat source. This unstable behaviour indicates that the thermodynamic equilibrium state in this system is strongly dependent on thermal transients and depicts reversible dynamics. Fig. 12b examines the Darcy's velocity changes at the same points. Under constant heat flux, the gas velocity slowly decreases and follows a stable pattern. The highest value is observed at point A, with an initial value of about 0.01665 $m.s^{-1}$, which gradually decreases to 0.0079 $m.s^{-1}$ at the end of the simulation. Points B and C also show a similar trend but with smaller values in magnitude, consistent with their radial position and weaker pressure gradient. In the stepwise heat flux method, a clear pulse behaviour in the velocity is observed. In the ON phases, the flow velocity increases significantly, especially at point A, which reaches a peak value of 0.03315 $m.s^{-1}$, and immediately decreases to values close to zero in the OFF phases. This response is fully consistent with the pressure changes and highlights the direct effect of the thermal input on the gas dynamics in the porous medium. These results illustrate a fundamental trade-off between thermal stability and peak dynamic performance in metal hydride systems. Under a constant heat flux, hydrogen pressure and flow increase gradually and uniformly across the bed, enabling steady-state operation with minimal spatial fluctuations. In contrast, the stepwise heating approach generates oscillatory behaviour in both pressure and velocity fields, especially near the heat source, as a result of alternating heating and relaxation phases. Although this transient response may initially appear unstable, it promotes higher instantaneous desorption rates and enhances hydrogen release during the active heating intervals. The absence of pressure stagnation during the OFF phases, along with the system's rapid recovery in subsequent heating cycles, confirms that gas flow remains consistent and reversible throughout. These results highlight the potential of pulsed thermal input to accelerate desorption effectively, provided that thermal application is carefully synchronized with system requirements. Ultimately, the decision between steady and stepwise heating strategies should align with specific operational goals: either favoring continuous, controlled output or maximizing hydrogen throughput in shorter cycles.

3.7. Energy consumption assessment

Fig. 13 provides a detailed comparison of the latent and sensible heat behaviour in magnesium hydride under two different thermal strategies. This figure not only shows the difference in desorption kinetics but also provides deeper insight into the energy consumption patterns and residual heat after the reaction, which are very important for evaluating the thermal efficiency of hydrogen storage cycles. In the constant heat flux case, the latent heat (related to the reaction) increases rapidly to about 260 $kJ.m^{-1}$ in the first few minutes. It then gradually decreases to about 230 $kJ.m^{-1}$ by the end of the 60-min simulation. This trend indicates that the desorption process is continuously active throughout the simulation, utilizing the supplied heat. At the same time, the sensible heat also increases steadily and gradually, eventually reaching about 70 $kJ.m^{-1}$. This gradual increase indicates that most of the input energy is spent on maintaining the endothermic reaction and gradually raising the bed temperature. However, since desorption continues throughout the cycle, there is no excess heat left to recover, and in this case, there is no separate energy-saving stage.

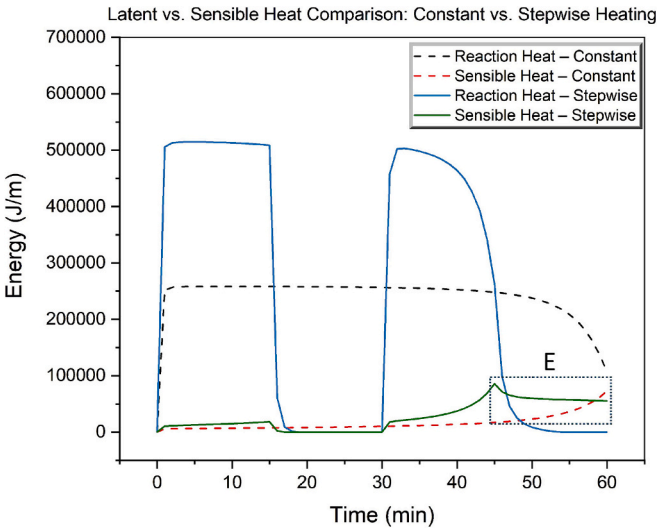

Fig. 13. Comparison of latent and sensible heat evolution under constant and stepwise heating strategies in the MgH_2 bed.

Unlike the stepwise heating strategy, in which heat is supplied in two separate 15-min ON-times with OFF-times in between, shows a completely different thermal behaviour. The latent heat curve in this case records two sharp peaks of about 510 $kJ.m^{-1}$, occurring in the intervals 0 to 15 and 30 to 45 min. After the second pulse, this curve quickly approaches zero, indicating that desorption is complete by 45 min, 15 min earlier than in the constant flux case. This faster behaviour can be attributed to the application of concentrated heat during the on phases, which increases the reaction rate. More importantly, the sensible heat profile in this case also increases in two steps; first, a slight increase during the first pulse and then a more significant increase during the second pulse. At the end of the desorption phase (at 45 min), the sensible heat reaches a maximum of about 80 $kJ.m^{-1}$ and then remains high (about 60 $kJ.m^{-1}$). This sensible energy after the end of the reaction, marked in box E in Fig. 13, represents a reserve of recoverable thermal energy that is no longer consumed for desorption. In contrast, in the constant flux case, there is no such stable level of sensible heat. This is because the energy is consumed as the reaction progresses and does not provide an opportunity for recovery. This thermal behaviour suggests that stepwise heating not only accelerates the desorption process but also provides a good opportunity for thermal recovery, a capability that is not available in the steady-state heating mode. Furthermore, by separating the reaction phase from the sensible heat accumulation phase, the stepwise approach allows for a more targeted use of energy and ensures that heat is applied exactly when it is chemically beneficial and effective. In summary, Fig. 13 shows that although both thermal strategies are capable of completing the desorption process, the stepwise approach does so with shorter reaction times, better heat matching to the reaction demand, and the possibility of thermal recovery. These advantages directly translate into reduced external heat requirements and improved overall thermal cycle efficiency, providing a rationale for using pulsed thermal control in the design of next-generation metal

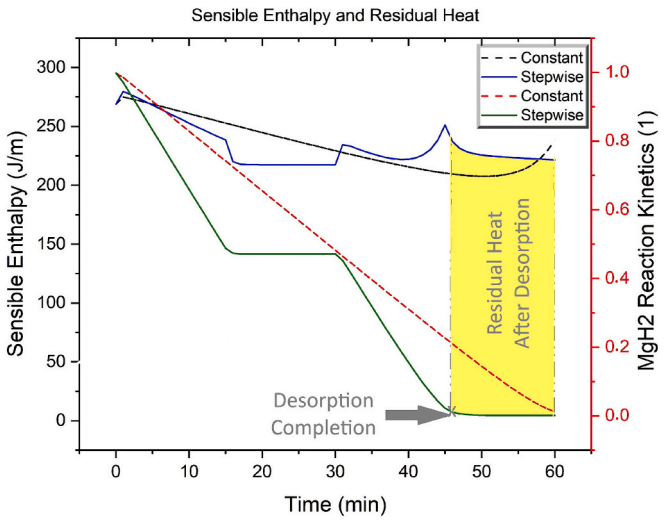

Fig. 14. Evolution of sensible enthalpy and reaction fraction under constant and stepwise heating.

hydride storage systems. Fig. 14 shows how two constant and stepwise heating strategies drive the process of hydrogen release and sensible heat accumulation in a magnesium hydride bed over 60 min. Starting with an initial sensible enthalpy of 268.7 J.m^{-1} and an initial reaction fraction x = 1, the curve for constant-flux heating (shown by the red dashed line) consumes heat continuously: over a full hour, u decreases linearly from 1.00 to about zero, while the sensible enthalpy gradually reaches 238.3 J.m^{-1}.

Since the reaction never stops, there is no opportunity to "store" thermal energy; any joule that enters the system is immediately used to maintain desorption or increase the bed temperature. In contrast, the stepwise heating curve (solid green line) divides the cycle into two 15-min on-periods separated by equal OFF-periods. In the first on-pulse, the sensible enthalpy increases, and u decreases to about 0.49 by minute 15; then in the OFF-phase (between minutes 15 and 30), x remains constant, even as the bed retains most of its heat at about 217 J.m^{-1}. The second pulse, occurring between 30 and 45 min, drives the reaction extent to nearly zero and completes the desorption process 15 min earlier than in the constant-flux case, while simultaneously increasing the sensible enthalpy to 251.1 J·m^{-1}. From minutes 45 to 60, in the absence of any energy-consuming reaction, this stored sensible heat slowly decreases from 251.1 to 221.5 J.m^{-1}. The shaded "yellow box" area under the curve during this time interval represents about 3.4 kJ/m of recoverable thermal energy, energy that would have been irreversibly lost in the constant flux mode. By synchronizing the heat transfer with the reaction kinetics in the bed, the stepwise approach not only reduces the cycle time by 25 % but also creates an inherent thermal buffer. At full scale for a 0.2 m radius vessel, this 3.4 kJ.m^{-1} of stored energy translates into about 0.7 MJ, which would be sufficient to preheat the incoming hydrogen or power a CHP loop. Thus, Fig. 14 clearly shows how pulse heating achieves more efficient energy management: it accelerates the ablation process, avoids unnecessary energy consumption, and provides an internal window for heat recovery, advantages that constant flux-based strategies cannot provide.

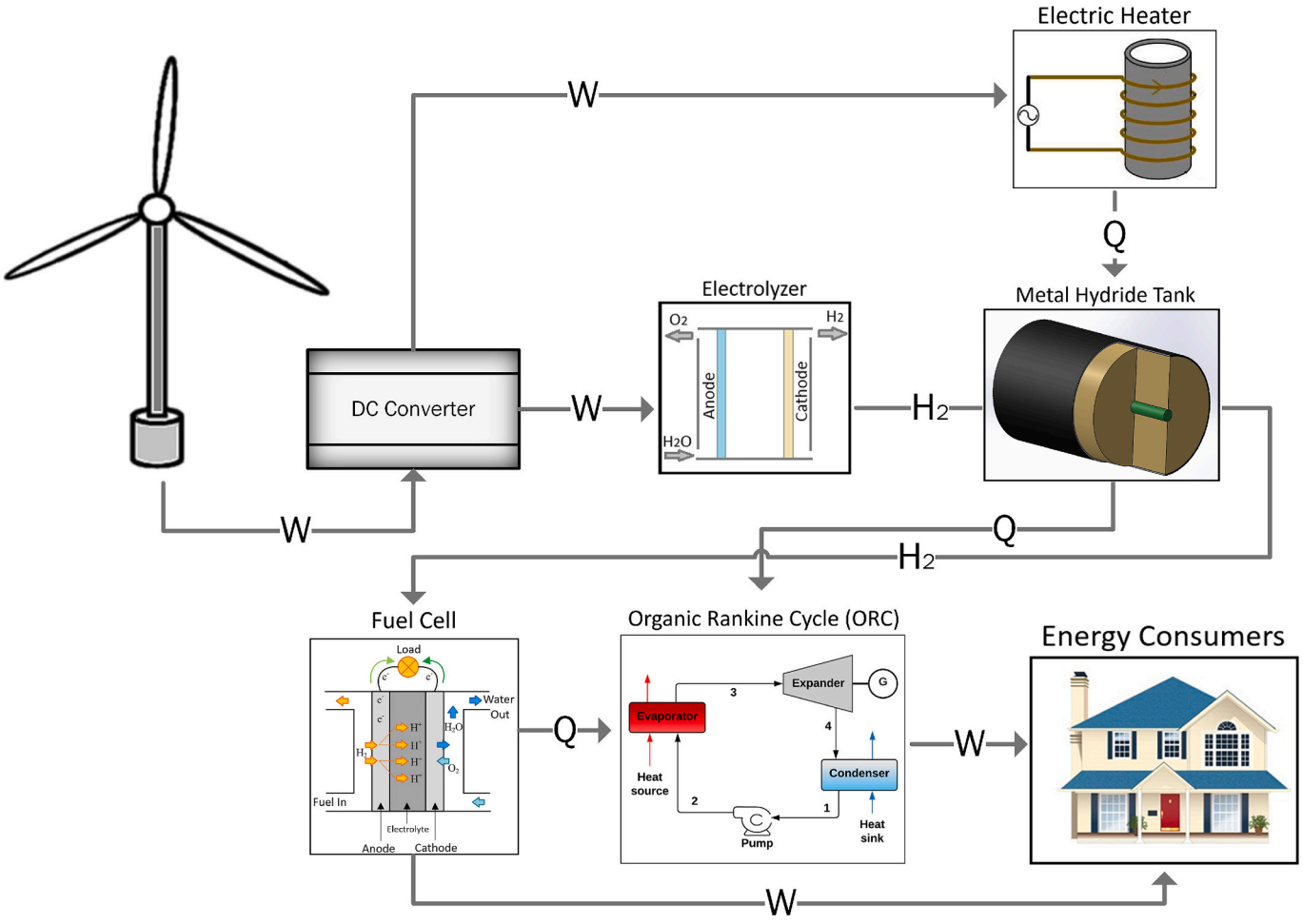

Fig. 15. Conceptual thermodynamic framework of the hydrogen storage system.

3.8. Thermal efficiency evaluation in constant and stepwise heat flux

In this section, a quantitative analysis of the thermal efficiency of the hydrogen desorption process in the MgH_2 bed under two different heat input strategies is presented. Before examining the efficiency in detail, Fig. 15 is introduced to provide a conceptual framework at the system level in which the proposed desorption module can operate.

Fig. 15 shows a renewable energy-based cycle. In this configuration, the electricity generated from a wind turbine is stabilized through a DC converter and directed to a proton exchange membrane (PEM) electrolyzer that produces hydrogen through water electrolysis. The produced hydrogen is stored in a MgH_2 tank, where the hydrogen is chemically absorbed and retained. When energy is required, the hydrogen is released through the thermal desorption process using an electric heater. The released hydrogen then enters a fuel cell that produces electricity and heat. As shown in the figure, the fuel cell exhaust heat can optionally be transferred to an organic Rankine cycle (ORC) to produce more power output and thus increase the overall system efficiency. It should be noted that the thermal efficiency analysis presented below focuses exclusively on the metal hydride tank and the electric heater, and does not include the full system shown in Fig. 15. After introducing this framework, the thermal performance of the desorption stage is quantitatively evaluated. The thermal efficiency (η) in this process is defined as the ratio of the useful output energy including the latent heat of desorption.

$$\eta = \frac{Q_{des} + Q_{sense,ret}}{Q_{in}} \tag{13}$$

In Eq.13, Q_{des} refers to the latent energy absorbed by the endothermic MgH_2 decomposition reaction, $Q_{sense,ret}$ represents the sensible heat retained in the hydride bed, and Q_{in} is the total thermal input. This formulation aligns with the standard thermodynamic definition of thermal efficiency as the ratio of useful energy output to input. Any energy not contributing to hydrogen desorption or retained as heat is considered waste. The quantitative values used in this analysis are summarized in Table 6, where both strategies are compared side by side under the same total heat input of 300 kJ.

According to the data in Table 6, the latent heat of desorption remains the same in both cases, equal to 40.9 kJ, as this value is directly related to the amount of hydrogen present and the enthalpy of reaction. In the continuous heating mode, no recoverable sensible heat remains in the bed after desorption, resulting in a thermal efficiency of 13.6 %. In contrast, in the pulsed heating configuration, 3.4 kJ of sensible heat is retained in the MgH_2 bed, increasing the total useful energy output to 44.3 kJ and improving the thermal efficiency to 14.8 %. Although the efficiency increase in this case is relatively limited (1.2 %), it demonstrates the advantage of using thermal cycles in preserving some of the energy that would otherwise be wasted. A sensitivity check considering heater thermal inertia, modeled as a first-order ramp with time constant τ_h, suggests that even conservative values (τ_h = 5–20 s) would reduce the average ON-segment heat flux by less than 2 % for 15 min pulses. Therefore, the reported relative efficiency improvement is expected to remain robust, although absolute values may be marginally lower in practice. This result supports an approach in which the use of stepwise heat flux can improve the thermal performance of the system; Not only through increased temperature uniformity and better control of the desorption process, but also through the possibility of recovering part of the stored heat. However, the overall efficiency of the system remains low, mainly due to thermal losses to the surroundings, emphasizing the need for advanced thermal management strategies and waste heat recovery techniques in MgH_2-based hydrogen storage systems.

Table 6
Thermal efficiency metrics for MgH_2 desorption under constant and pulsed heating.

Parameter	Formula	Constant Heating	Pulsed Heating
Input energy Q_{in} (kJ)	$q''At$	300	300
Latent heat Q_{des} (kJ)	$Q_{des} = \Delta H_{des} n H_2$	40.9	40.9
Retained sensible heat $Q_{sense,ret}$ (kJ)	$Q_{sense,ret} = \rho_{bed} V_{bed} c_p (T_{final} - T_{initial})$	0.0	3.4
Useful output (kJ)	$Q_{use} = Q_{des} + Q_{sense,ret}$	40.9	44.3
Thermal efficiency η (%)	$\eta = \frac{Q_{use}}{Q_{in}}$	13.6	14.8

3.9. Comparative performance analysis with existing thermal management methods

A comparison was carried out between the proposed stepwise (pulsed) heating strategy and several established thermal enhancement techniques, including thermochemical storage systems (TCSS) [26], phase change materials (PCM) [49], metal foams [50], fins [51], and internal heat exchangers [11]. The results, summarized in Fig. 16, show that conduction-based methods such as metal foams and heat exchangers achieve both large reductions in desorption time and substantial increases in average bed temperature. For example, the heat exchanger case reaches the highest average temperature increase of approximately 38.7 % above the baseline, accompanied by a 38.1 % reduction in desorption time. Similarly, metal foams deliver a 40.6 % temperature gain with a 35.7 % faster desorption time. These improvements, however, come at the expense of significant additional heat transfer into the bed and the inclusion of complex internal structures.

By contrast, the stepwise heating method achieves a remarkable 25 % reduction in desorption time while raising the average bed temperature by only about 3 %. This temperature gain is the lowest among all methods, yet the improvement in desorption time is comparable to more heat-intensive techniques. This suggests that the total heat flux input is considerably lower, making the process more energy efficient. The maximum performance gain in desorption time across all methods is observed for the heat exchanger case (38.1 %), while the minimum is seen for TCSS (11 %). In terms of temperature gain, metal foam provides the maximum (40.6 %) and stepwise heating the minimum (~3 %). This combination of modest temperature rise and significant desorption acceleration makes stepwise heating particularly attractive for applications where energy efficiency, system simplicity, and minimal design changes are prioritised over achieving the maximum possible bed temperature. To further contextualize the performance trends observed in

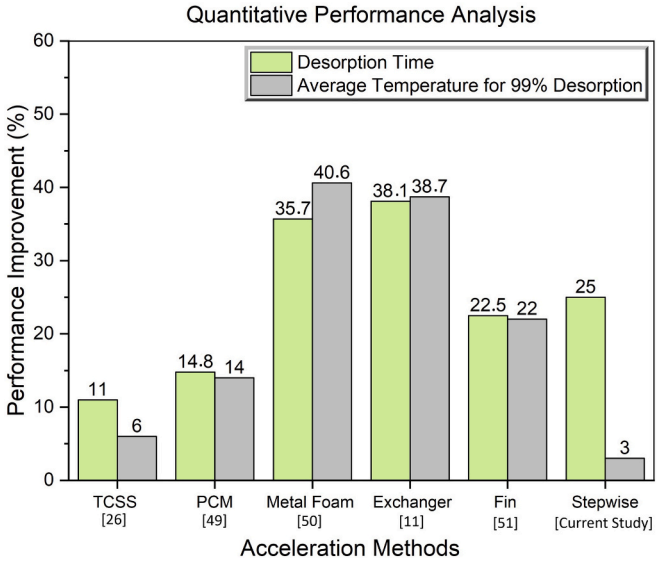

Fig. 16. Quantitative performance improvement of different acceleration methods.

Fig. 16, Table 7 presents a qualitative comparison of the examined enhancement methods. This table not only reflects their relative effectiveness in accelerating desorption but also considers broader aspects such as energy management efficiency, installation complexity, and practical feasibility. Conduction-based solutions like metal foams and internal heat exchangers consistently deliver high or very high performance, but they demand significant structural modifications, carry higher fabrication costs, and often add mass or reduce active hydride volume. PCM-based systems and TCSS offer moderate gains with smoother temperature profiles and easier integration, but their acceleration effect is more limited.

By contrast, the proposed stepwise (pulsed) heating method stands out as combining high desorption performance with very high energy efficiency, while avoiding the fabrication complexity and cost of embedded conduction enhancers. Its ability to achieve strong acceleration with only a minimal increase in average bed temperature highlights an important advantage: the method delivers substantial hydrogen release rates without the heavy thermal input or structural redesigns that conduction-based approaches require. This efficiency not only reduces operational energy demand but also improves system sustainability, making it highly attractive for portable, modular, or renewable-powered hydrogen storage systems where energy availability is limited. Furthermore, the absence of additional internal components preserves the full active volume of the hydride bed, simplifies manufacturing, and enhances reliability by eliminating potential failure points. Taken together, these characteristics suggest that stepwise heating can serve as both a performance-boosting and cost-saving strategy, offering a balanced solution for practical metal hydride applications across a wide range of scales.

4. Conclusions

This study investigated the hypothesis that a pulsed wall heat flux could help overcome the intrinsic thermal conductivity limitations of magnesium hydride (MgH_2), which hinder hydrogen desorption. A validated finite element model, showing less than 1 % error compared to the experimental data from Chaise et al. [46] and Lutz et al. [20] were used to simulate heat transfer and gas dynamics under varying thermal input strategies. By alternating the wall flux between 0 and 13.4 $kW{\cdot}m^{-2}$ in 15-min ON/OFF cycles, the pulsed approach significantly enhanced system performance compared to conventional constant flux. The results demonstrated that:

1. The complete desorption time was reduced from 60 to 45 min (a 25 % improvement), while the internal temperature field remained stable and hot spots were avoided.
2. The pulsed heating enhancement can be attributed to a dynamic λ-feedback: each heating pulse converts MgH_2 to metallic Mg (higher λ), which improves heat transfer for subsequent pulses and accelerates desorption.
3. The radial temperature gradient decreased by approximately 40 %, and the wall temperature was maintained below 661 K.
4. Around 3.4 $kJ{\cdot}m^{-3}$ of sensible heat was retained in the bed at the end of desorption, an energy buffer not available in constant-flux strategies.

Further analysis indicated that improving MgH_2's thermal conductivity beyond 4.2 $W{\cdot}m^{-1}{\cdot}K^{-1}$ did not lead to continued performance gains, as the system became limited by gas-phase transport and surface kinetics. This finding suggests that pulsed heating alone may offer performance comparable to more complex solutions, such as embedded fins or metal foams, but without compromising usable storage volume or increasing system complexity. This work introduces the concept of "heat flux sequencing" a simple yet potentially powerful strategy in thermal management, as a standalone tool to enhance desorption performance. While promising, further investigation is needed to confirm these benefits under experimental conditions and at practical scales. Future research directions include:

- Experimental validation of the model in a laboratory-scale cylindrical MgH_2 reactor equipped for both constant and pulsed wall heating, with temperature and pressure sensors to capture spatio-temporal profiles and verify predicted desorption kinetics and efficiency gains.
- Integration of adaptive pulsed heating with phase-change or thermochemical storage to recover retained sensible heat.
- Extension to 3D geometries and larger-scale systems to evaluate performance under realistic operating conditions.

Altogether, these efforts aim to bridge the gap between numerical modeling and practical application, potentially enabling lighter, more efficient hydrogen storage systems, and could extend the utility of pulsed thermal input strategies to other hydride materials and thermochemical processes.

CRediT authorship contribution statement

Davoud Abdi Lanbaran: Writing – review & editing, Writing – original draft, Methodology, Investigation, Formal analysis, Conceptualization. **Pouria Farokhi Kojour:** Visualization, Investigation, Data curation. **Chao Wang:** Project administration. **Chuang Wen:** Writing – review & editing. **Zhen Wu:** Writing – review & editing, Conceptualization. **Mi Tian:** Writing – review & editing, Supervision, Project administration. **Bo Li:** Writing – review & editing, Writing – original draft, Supervision, Resources, Project administration, Methodology, Funding acquisition, Formal analysis, Data curation.

Table 7
Thermal efficiency metrics for MgH_2 desorption under constant and pulsed heating.

Method	Material(s) Used	Energy Management Efficiency	Installation / Fabrication Difficulty	Cost Level	Other Notes / Benefits
TCSS [26]	MgH_2 + MgO	Moderate	Low – can be retrofitted externally	Low	Provides supplementary heat via exothermic hydration; no major redesign needed.
PCM [49]	Mg_2Ni with PCM shell	Moderate–High (buffers heat peaks)	Moderate – requires PCM containment	Moderate	Smooths temperature profile; improves thermal uniformity; adds mass and volume.
Metal Foam [50]	MgH_2 + Aluminum foam	High	Moderate – requires embedding foam into the MH bed	High	Strong thermal conduction boost; lightweight but expensive material.
Heat Exchanger [11]	MgH_2 + cylindrical tubes	High	Highly complex fabrication and integration	High	Maximizes heat transfer; proven design; increases system weight and cost.
Fins [51]	MgH_2 + aluminum fins	Moderate–High	Moderate – machining and insertion required	Moderate	Reliable conduction path, occupies MH volume; scalable design.
Stepwise (Pulsed) Heating	MgH_2	Very High (low heat input for high output)	Low – uses external control, no bed modification	Low	Achieves rapid desorption with minimal temperature rise; highly energy-efficient; ideal for retrofit without structural change.

Declaration of competing interest

The authors declare that they have no known competing financial interests or personal relationships that could have appeared to influence the work reported in this paper.

Acknowledgments

This work was supported by the National Natural Science Foundation of China (No. 52176203).

Data availability

Data will be made available on request.

References

[1] Gharanli S, Gharib A, Moharramnejad M, Karim A, Malekshah RE, Karimi F, et al. Environmentally friendly nickel-based nanocomposites for energy storage: a review of supercapacitor and battery-type mechanisms. J Energy Storage 2025;122:116509.
[2] Wang Z, Lao G. Hydrogen production from renewable sources: bridging the gap to sustainable energy and economic viability. Int J Hydrog Energy 2025;117:121–34.
[3] Muhammed NS, Gbadamosi AO, Epelle EI, Abdulrasheed AA, Haq B, Patil S, et al. Hydrogen production, transportation, utilization, and storage: recent advances towards sustainable energy. J Energy Storage 2023;73:109207.
[4] Hsu CY, Kostoglou N, Mitterer C, Rebholz C, Chang CK, Chuang YC, et al. Enhanced dehydrogenation and regeneration behaviour of LiBH4–LiAlH4–MgCl2 in nanoporous carbons. Int J Hydrog Energy 2025;106:712–22.
[5] Kumar A, Muthukumar P, Sharma P, Kumar EA. Absorption based solid state hydrogen storage system: a review. Sustain Energy Technol Assess 2022;52:102204.
[6] Dubey SK, Kumar KR. Charging and discharging analysis of thermal energy using magnesium nickel hydride based thermochemical energy storage system. Sustain Energy Technol Assess 2022;52:101994.
[7] Kim DM, Han DJ, Heo TW, Kang S, Wood BC, Lee J, et al. Enhancement of effective thermal conductivity of rGO/Mg nanocomposite packed beds. Int J Heat Mass Transf 2022;192:122891.
[8] Lanbaran DA, Wang C, Wen C, Wu Z, Li B. Modeling the impact of temperature-dependent thermal conductivity on hydrogen desorption from magnesium hydride. Int J Hydrog Energy 2025;138:491–508.
[9] Li Q, Lu Y, Luo Q, Yang X, Yang Y, Tan J, et al. Thermodynamics and kinetics of hydriding and dehydriding reactions in Mg-based hydrogen storage materials. J Magnesium Alloys 2021;9(6):1922–41.
[10] Lang J, Eagles M, Conradi MS, Huot J. Hydrogenation rate limiting step, diffusion and thermal conductivity in cold rolled magnesium hydride. J Alloys Compd 2014;583:116–20.
[11] Larpruenrudee P, Bennett NS, Gu Y, Fitch R, Islam MS. Design optimization of a magnesium-based metal hydride hydrogen energy storage system. Sci Rep 2022;12(1):13436.
[12] Malka IE, Bystrzycki J. The effect of storage time on the thermal behaviour of nanocrystalline magnesium hydride with metal halide additives. Int J Hydrog Energy 2014;39(7):3352–9.
[13] Albert R, Urbanczyk R, Felderhoff M. Thermal conductivity measurements of magnesium hydride powder beds under operating conditions for heat storage applications. Int J Hydrog Energy 2019;44(55):29273–81.
[14] Li S, Yang X, Hou J, Du W. A review on thermal conductivity of magnesium and its alloys. J Magnesium Alloys 2020;8(1):78–90.
[15] Bennett CM, Patman AJ, Milanese C, Eastwick CN, Walker GS. Effect of powder characteristics for a magnesium based metal hydride store. Int J Hydrog Energy 2014;39(34):19646–55.
[16] Thongtan P, Thiangviriya S, Utke O, Utke R. MgH2-based hydrogen storage tank: kinetics, reversibility, and MWCNTs content. J Phys Chem Solids 2022;163:110578.
[17] Popilevsky L, Skripnyuk VM, Amouyal Y, Rabkin E. Tuning the thermal conductivity of hydrogenated porous magnesium hydride composites with the aid of carbonaceous additives. Int J Hydrog Energy 2017;42(35):22395–405.
[18] Kumar EA, Madaria Y, Babu KS, Murthy SS. Influence of effective thermal conductivity on hydrogen sorption in Mg-LaNi4. 6Al0. 4 composite hydride beds for thermal energy storage. Thermal Sci Eng Progress 2020;19:100653.
[19] Yoshida K, Noda S, Hanada N. Heat supply to and hydrogen desorption from magnesium hydride in a thermally insulated container with hot gas flow. Chem Eng J 2024;491:152070.
[20] Lutz M, Bhouri M, Linder M, Bürger I. Adiabatic magnesium hydride system for hydrogen storage based on thermochemical heat storage: numerical analysis of the dehydrogenation. Appl Energy 2019;236:1034–48.
[21] Malleswararao K, Aswin N, Kumar P, Dutta P, Murthy SS. Experiments on a novel metal hydride cartridge for hydrogen storage and low temperature thermal storage. Int J Hydrog Energy 2022;47(36):16144–55.
[22] Lamrani B, Alqahtani RT, Ajbar A, Kousksou T. Resistance-capacitance dynamic model for hydrogen storage in metal hydrides with phase change material as thermal management system. Energy Convers Manag 2025;X:101007.
[23] Zamengo M, Ryu J, Kato Y. Thermochemical performance of magnesium hydroxide–expanded graphite pellets for chemical heat pump. Appl Therm Eng 2014;64(1–2):339–47.
[24] Neves AM, Puszkiel J, Capurso G, von Colbe JB, Klassen T, Jepsen J. Development of a new approach for the kinetic modeling of the lithium reactive hydride composite (Li-RHC) for hydrogen storage under desorption conditions. Chem Eng J 2023;464:142274.
[25] Ye Y, Zhu H, Cheng H, Miao H, Ding J, Wang W. Performance optimization of metal hydride hydrogen storage reactors based on PCM thermal management. Appl Energy 2023;338:120923.
[26] Shi T, Xu HJ, Ke HB, Zhao CY. Thermal transport of charging/discharging for hydrogen storage in a metal hydride reactor coupled with thermochemical heat storage materials. Energy Convers Manag 2022;273:116421.
[27] Zhu Z, Bao Z, Wu D. Optimization of the content distribution of expanded natural graphite in a multilayer metal hydride bed for thermochemical heat storage. Appl Therm Eng 2022;216:119115.
[28] Chen J, Bie H, Wang J, Sun B. Optimization operation method for hydrogen-compressed natural gas-integrated energy systems considering hydrogen-thermal multi-energy inertia. Res Eng Des 2025;25:103652.
[29] Mou X, Bao Z, Huang W. Performance investigation of metal hydride reactor equipped with helically coiled heat exchanger during hydrogen absorption and desorption. Thermal Sci Eng Progress 2023;38:101656.
[30] Shi J, Gao J, Xiong L, Zhang Z, Han Z, Gao B. Study on the impact of heat exchange structures on hydrogen storage performance in magnesium-based hydrogen storage reactors. Int J Hydrog Energy 2025;112:468–81.
[31] Wu Z, Yang F, Zhang Z, Bao Z. Magnesium based metal hydride reactor incorporating helical coil heat exchanger: simulation study and optimal design. Appl Energy 2014;130:712–22.
[32] Atalmis G, Sattarkhanov K, Demiralp M, Kaplan Y. The effect of expanded natural graphite added at different ratios of metal hydride on hydrogen storage amount and reaction kinetics. Int J Hydrog Energy 2024;51:256–65.
[33] Thiangviriya S, Thongtan P, Thaweelap N, Plerdsranoy P, Utke R. Heat charging and discharging of coupled MgH2–LaNi5 based thermal storage: cycling stability and hydrogen exchange reactions. Int J Hydrog Energy 2024;49:59–66.
[34] Jiang Y, Si N, Jiang W, Wang Z, Zhang H. FeNiCu-based composite catalyst for hydrogen storage in MgH2. Chem Eng J 2024;499:156449.
[35] Elman R, Kudiiarov V, Sayadyan A, Pushilina N, Leng H. Performance improvement of magnesium-based hydrogen storage tanks by using carbon nanotubes addition and finned heat exchanger: numerical simulation and experimental verification. Int J Hydrog Energy 2024;92:1375–88.
[36] Eisapour AH, Fung AS, Shafaghat A, Khosravi K. Enhancing hydrogen storage efficiency in metal hydride tanks through conical heat exchangers and phase change material integration. Int J Hydrog Energy 2025;109:1090–107.
[37] Su JW, Tang XY, Bai XS, Yang WW, Zhang JF, Qu ZG. Review on thermal design and thermal management for metal hydride reactors: current status and future development. Int J Hydrog Energy 2025;114:295–311.
[38] Xu H, Shi T, Xu H, Yu G. Regulation and optimization of solid-state hydrogen storage process in thermochemical reactors with metal hydride by using gradient metal foams. Appl Therm Eng 2025;264:125464.
[39] Shi T, Xu H. Integration of hydrogen storage and heat storage in thermochemical reactors enhanced with optimized topological structures: charging process. Appl Energy 2022;327:120138.
[40] Qureshi ZA, Ali HM, Khushnood S. Recent advances on thermal conductivity enhancement of phase change materials for energy storage system: a review. Int J Heat Mass Transf 2018;127:838–56.
[41] Kapischke J, Hapke J. Measurement of the effective thermal conductivity of a Mg–MgH2 packed bed with oscillating heating. Exp Thermal Fluid Sci 1998;17(4):347–55.
[42] Bhouri M, Bürger I. Numerical investigation of H2 absorption in an adiabatic high-temperature metal hydride reactor based on thermochemical heat storage: MgH2 and Mg (OH) 2 as reference materials. Int J Hydrog Energy 2017;42(26):16632–44.
[43] Zimmerman WBJ. Introduction to COMSOL multiphysics. In: Multiphysics Modeling with Finite Element Methods; 2006. p. 1–26.
[44] Wakao N, Kaguei S, Funazkri T. Effect of fluid dispersion coefficients on particle-to-fluid heat transfer coefficients in packed beds: correlation of Nusselt numbers. Chem Eng Sci 1979;34(3):325–36.
[45] Wang CS, Brinkerhoff J. Advances in mathematical modeling of hydrogen adsorption and desorption in metal hydride beds with lattice Boltzmann method. Int J Hydrog Energy 2020;45(56):32179–95.
[46] Chaise A, De Rango P, Marty P, Fruchart D. Experimental and numerical study of a magnesium hydride tank. Int J Hydrog Energy 2010;35(12):6311–22.
[47] Rickman SL, Ungar EK. A physics-based temperature stabilization criterion for thermal testing. In: 25th Aerospace Testing Seminar; 2009, October (no. LF99-8634).
[48] Lewis RW, Nithiarasu P, Seetharamu KN. Fundamentals of the finite element method for heat and fluid flow. John Wiley & Sons; 2004.

[49] Ye Y, Ding J, Wang W, Yan J. The storage performance of metal hydride hydrogen storage tanks with reaction heat recovery by phase change materials. Appl Energy 2021;299:117255.

[50] Bai XS, Yang WW, Tang XY, Dai ZQ, Yang FS. Parametric optimization of coupled fin-metal foam metal hydride bed towards enhanced hydrogen absorption performance of metal hydride hydrogen storage device. Energy 2022;243:123044.

[51] Bao Z, Yang F, Wu Z, Cao X, Zhang Z. Simulation studies on heat and mass transfer in high-temperature magnesium hydride reactors. Appl Energy 2013;112:1181–9.